In-situ generation of H_2O_2 using Fenton-like AC-Fe-Cu composite for degradation of Methylene Blue

By

Sumaiya Hussain

Registration No. 00000327910

Supervisor: Dr. Muhammad Zeeshan Ali Khan

Institute of Environmental Sciences and Engineering (IESE)

School of Civil and Environmental Engineering (SCEE)

National University of Sciences and Technology (NUST)

Islamabad, Pakistan

2022

In-situ generation of H_2O_2 using Fenton-like AC-Fe-Cu composite for degradation of Methylene Blue

By

Sumaiya Hussain
Registration No. 00000327910

A thesis submitted in partial fulfillment of requirements for the degree of

Master of Science

in

Environmental Engineering

Institute of Environmental Sciences and Engineering (IESE)
School of Civil and Environmental Engineering (SCEE)
National University of Sciences and technology (NUST)
Islamabad, Pakistan

2022

APPROVAL CERTIFICATE

It is certified that the contents and form of the thesis entitled **"In-situ generation of H_2O_2 using Fenton-like AC-Fe-Cu composite for degradation of Methylene Blue"** submitted by Ms. Sumaiya Hussain has been found satisfactory for partial fulfillment of the requirements of the degree of Master of Science in Environmental Engineering.

Supervisor: ____________________

Dr. Muhammad Zeeshan Ali Khan

Associate Professor

IESE, SCEE, NUST

Member: _______________________

Dr. Waqas Qamar Zaman

Assistant Professor

IESE, SCEE, NUST

Member: _______________________

Dr. Muhammad Ali Inam

Assistant Professor

IESE, SCEE, NUST

THESIS ACCEPTANCE CERTIFICATE

It is certified that the contents and forms of the thesis entitled **"In-situ generation of H_2O_2 using Fenton-like AC-Fe-Cu composite for degradation of Methylene Blue"** submitted by Ms. Sumaiya Hussain, Registration No. 00000327910 is found complete in all respects as per NUST Regulations, is free of plagiarism, and mistakes and is accepted as partial fulfilments for award of MS degree. It is further certified that necessary modifications as pointed out by GEC members of the scholar have been included in the said thesis

Supervisor: ____________________

Dr. Muhammad Zeeshan Ali Khan

Associate Professor

IESE, SCEE, NUST

Head of Department: ___________________

Date: ___________________

Dean/Principal: ___________________

Date: ___________________

DECLARATION

I certify that research work titled **"In-situ generation of H_2O_2 using Fenton-like AC-Fe-Cu composite for degradation of Methylene Blue"** is my own work. The work has not been presented elsewhere for assessment. Where material has been used from other sources, it has been properly acknowledged and referred.

Sumaiya Hussain

00000327910

PLAGIARISM CERTIFICATE

I certify that this research work titled as **"In-situ generation of H_2O_2 using Fenton-like AC-Fe-Cu composite for degradation of Methylene Blue"** is my own work. Thesis has significant new work as compared to already published or under consideration to be published elsewhere. The thesis has been checked using TURNITIN and found within limits as per HEC plagiarism Policy and instructions issued from time to time.

Sumaiya Hussain

00000327910

Signature: ___________________

Supervisor: ___________________

Date: ___________________

DEDICATION

“This thesis is dedicated to all the marvelous people in my life whose continuous and untiring support instilled in me enough dedication to reach this goal. I shall forever be grateful to my family and friends for believing in me and never giving up on me”

ACKNOWLEDGEMENTS

First of all, I would like thank Allah Almighty for enabling me to pursue this degree and then by His grace, concluding it.

I would like to express my deepest appreciation to my supervisor, Dr. Zeeshan Ali Khan for bringing the weight of his considerable experience and knowledge to this research. His continuous support, guidance and invaluable wisdom carried me through all the stages of the research and for that I shall always be grateful.

I would also like to express special thanks to my GCE members, Dr. Waqas Qamar Zaman and Dr. Muhammad Ali Inam for their generous support and understanding while undertaking my research. It would not have been possible without their constant belief in me.

Sumaiya Hussain

Table of Contents

List of Figures

List of Tables

Abstract

A novel Fenton-like AC-Fe-Cu composite was synthesized characterized and optimized to accomplish mineralization of Methylene Blue. This composite was synthesized at different temperatures and mass ratios of copper to select the optimum synthesis temperature and effective mass ratio of copper. The optimum synthesis temperature was 500ºC and effective mass ratio of AC:Fe:Cu was 3:1:0.25. This composite was used to run a series of batch experiments. Internal micro-electrolysis took place between Fe^0, Cu^0 and carbon which facilitated reduction of molecular oxygen (O_2) to hydrogen peroxide (H_2O_2). H_2O_2 has an oxidation potential of 1.8V hence, it is capable of efficiently degrading organic pollutants. This H_2O_2 was further reduced to hydroxyl radical ($^{\bullet}OH$) by Fenton-like reaction between Fe^{2+} and Cu^+ and carbon. Hydroxyl radical has an oxidation potential of 2.8V, thereby enhancing the oxidizing ability of the whole system. Characterization results showed successful synthesis of composite. The BET surface area of the AC-Fe-Cu composite was 172.94 m^2/g. The maximum removal efficiency of MB using this composite was 99.6% at composite dosage of 1g/L, pH of 1, MB concentration of 50mg/L and reaction time 2 hours. In-situ H_2O_2 generation was 12mg/L in 120 mins. Composite gave the best results at a composite dosage of 1g/L, pH 4 and a MB concentration of 50mg/L.

1 Introduction

The global human population will reach 8 billion by November 2022 (“World Popul. Prospect.,” 2022). Out of those 8 billion people, around 1400 million people (of which around half a million are children) are currently residing in the areas of high water scarcity (Wash, 2002). 45 major cities and 3 million people will be living in areas experiencing extremely high water stress in less than years (Mitlin et al., 2019). Earth’s freshwater resources, which are less than 3 percent, are highly threatened. (US Geological Survey, 2021). To worsen the situation, poor management, inadequate utilization, contamination of freshwater supplies and over extraction of groundwater have aggravated the water crisis. Moreover, there is a huge rise in water demand due to rapid increase in population, urban sprawl and industrialization. Demand for food and energy also increases due to increase in population which also leads to increase in water demand (Biswas & Tortajada, 2018). At the current rate of population growth, there will be a 20 to 30 percent increase in global water demand by the year 2050.

Another factor contributing to water crisis is climate change. One of the impacts of Climate change is the variation in weather patterns causing a drastic rise in water demand. Changes in climate change are mostly associated with water like rising sea levels, droughts and floods and such weather events can damage essential water and sanitation infrastructure and services. Due to climate change, sea levels are rising more than expected causing saltwater intrusion which will contaminate river and groundwaters. Rapid melting of glaciers is another consequence of climate change which alters the river course in the downstream areas, increasing the frequency and intensity of floods and damaging infrastructure like dams, decreasing the amount of water available for consumption and use. These events along with amplified agriculture industrialization and urbanization have aggravated the water crisis all over the world but more specifically in developing countries (UNEP, 2016).

Water scarcity is an issue faced all over the world as water is a finite resource and decrease in water resources is causing conflicts among communities leading to mass migrations. In some areas, people have to travel for miles to find portable water and many migrate to urban areas, putting more pressure on already strained water resources. This hinders the sustainable development of the communities (Wash, 2002).

The arid and semi-arid countries are the ones most affected by water scarcity. In regions facing water scarcity, industrialization and urbanization have caused severe pressure on local water resources. To address this situation sustainable solutions, need to be implemented to cater the problem of water scarcity. One of the most promising practices is wastewater reuse (Pereira et al., 2002). The most traditional and feasible purpose for wastewater reuse is irrigation. Although since past many years, technological advances have allowed for effective treatment of wastewater that is suitable for use other than agricultural purposes.

Wastewater effluent from leather, rubber, textile, paper cosmetics and synthetic detergent industries contains harmful contaminants like heavy metals and dyes, which can cause serious environmental and health problems if they are not treated properly. The European Commission describes textile industry as “one of the longest and most complicated industrial chains in manufacturing industry” (The European Commission, 2003). The manufacturing process in a textile industry starts with natural raw material like cotton, wool, and flax or synthetic raw material, produced from petroleum derivatives, like polyesters and polyamides, etc. The raw materials are then processed via different processes like spinning, weaving and knitting etc resulting in production of threads and textiles which then go through bleaching, dyeing, mercerizing and washing (Holkar et al., 2016)(Bhatia et al., 2017). Every process in "textile industry chain" either uses nonrenewable energy or releases harmful pollutants into the environment (The European Commission, 2003). Although, the biggest threat posed by the textile industry is its huge water consumption and subsequently the production of highly toxic wastewater (Bhatia et al., 2017). The most water consuming processes are the wet processes employed for dying. They also produce most amount of wastewater during production of textiles (Holkar et al., 2016).

Wastewater effluent from textile industry has high COD, ranging from 150 - 10,000 mg/L, BOD ranging from 100-4000 mg/L, a pH of 6-10 and color content in the range 50-2500. (Asghar et al., 2015). Textile effluent has variable and complex composition hence a lot of treatment methodologies in different configurations are employed for treatment of these contaminants such as conventional physical treatment processes (coagulation/ flocculation, membrane filtration), biological treatment processes, membrane processes and Advanced Oxidation Processes (AOPs) (The European Commission, 2003)(Ribeiro et al., 2017)(Yukseler et al., 2017). The physical and membrane processes change the phase of the pollutant or concentrate them in one phase whereas biological process and AOPs can either degrade or completely eradicate the contaminants. In biological processes, pollutants are oxidized or reduced through metabolic capabilities of bacteria, fungi and algae, etc. (Bhatia et al., 2017)(Khandare & Govindwar, 2015). Processes which occur in nature are accelerated when suitable conditions are met. They are commonly used in bioreactors, with suitable aeration and agitation equipment. Sometimes wetlands are also used for this. Biodegradation methodologies are generally considered as economical (Khandare & Govindwar, 2015)(Punzi et al., 2015) – in terms of operation costs. Relative to the equipment used, the investment cost could be high. Bioprocesses transform only biodegradable compounds which is a limitation. Furthermore, the existence of toxic materials may slowdown biological processes and avoid the usage of microorganisms (Ganzenko et al., 2014). Even though the biological treatment of wastewater is a widely used solution, the methods involved are being improved constantly. AOPs include many different techniques including Fenton oxidation, ozonation, ionizing radiation technology, sulfate radical-based technology, UV/chlorine advanced oxidation, and the like (Liu et al., 2021). All these techniques produce strong oxidizing agents which react through electron transfer or radical addition. Resultantly, they are able to degrade long chained chemical structures, like bio refractory compounds which are produced due to industrial activities and are difficult to degrade using biological processes (Arslan & Balcioglu, 2001).

1.1 Advanced Oxidation Processes

Advanced oxidation processes (AOPs) making use of ROS for mineralization of pollutants were initially employed during the 1980s to accomplish treatment of drinking water. (Glaze, 1987). Since then AOPs have been widely used to accomplish mineralization of various organic pollutants as they can promptly breakdown the refractory organic contaminants and eliminate some inorganic pollutants as well. Unlike common oxidants such as ozone and chlorine that are employed for purification of water, AOPs are only used to degrade organic and inorganic pollutants in water and wastewater. While studies have been conducted for the use of AOPs as disinfectants, (Cho et al., 2005)(Ikai et al., 2010), they have been rarely used to as disinfectants because the radicals have half-life of microseconds (Tchobanoglous et al., 2011). The AOPs are employed for mineralization of pollutants as they are strong oxidants successfully accomplish the degradation of harmful contaminants, to decrease their toxicity by producing non-toxic end products (Huang et al., 1993).

AOPs employing $^{\bullet}OH$ (oxidation potential 2.8V) are highly preferred now because of their high oxidizing ability (Wang & Xu, 2012). Methods used in AOPs include, photocatalysis, ozonation, electrochemical oxidation, Fenton and Fenton-like processes as shown in Figure 1.1. Even though these methods use different reaction mechanisms, they all are similar in a way that they employ strong oxidants for mineralization of pollutants.

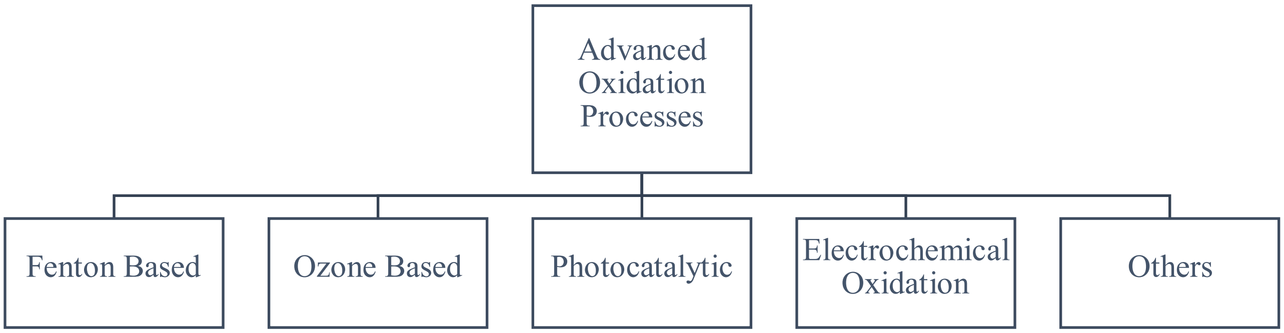

Figure 1.1: Different advanced oxidation processes

Among all the AOPs, Fenton based processes have gained attention as the process is capable of generating hydroxyl radical in acidic environment. The process can be demonstrated by equation 1:

$$\text{“}Fe^{2+} + H_2O_2 \rightarrow Fe^{3+} + {}^{\bullet}OH + OH^{-}\text{”} \qquad \textbf{(1)}$$

1.2 Fenton and Fenton-like Reaction

As compared to other AOPs, Fenton/Fenton-like processes that decompose H_2O_2 to generate ${}^{\bullet}OH$ have been widely employed and studied due to a number of reasons including simple and easy operating conditions and high concentration of ${}^{\bullet}OH$ formation (Cheng et al., 2018). In conventional Fenton/Fenton-like process, of hydrogen peroxide is typically supplied in bulk but the effectiveness of H_2O_2 consumption in this case is very low. Moreover, storage, transportation and handling of H_2O_2 in high concentrations are costly due to which the process has become potentially dangerous and economically challenging (Asghar et al., 2015)(Pi et al., 2020). In order to cater these problems, Fenton/Fenton-like process capable of generating in-situ H_2O_2 by activating molecular oxygen has gained much attention because of a number of reasons including easy availability of O_2 and safe operating conditions unlike H_2O_2. This novel Fenton/ Fenton-like process uses O_2 to produce in-situ generated H_2O_2 by reduction. H_2O_2 is further reduced to produce $^{\bullet}OH$ radical by employing Fenton/Fenton-like composites. Reduction of O_2 for production of in-situ H_2O_2 plays a significant part for treatment of emergent pollutants.

Many studies investigated the chemical activation of O_2 employed for production of H_2O_2 like by using metal or metal-free reducers. Transition metal composites and zero-valent metals including zero-valent iron, zinc, aluminum, magnesium and copper have been recently used for activation of O_2 for in-situ generation of H_2O_2. Some zero-valent metals like iron, and copper are capable of simultaneously reducing H_2O_2 to $^{\bullet}OH$ along with reduction of O_2 to H_2O_2 (Noubactep, 2009)(H. Zhang et al., 2012). However, other ZVMs, like magnesium and zinc, used in Fenton/Fenton-like Processes, can only accomplish reduction of O_2 to H_2O_2. Due to this reason it becomes necessary to use Fenton/Fenton-like composites do reduce the in-situ generated H_2O_2 to $^{\bullet}OH$. Therefore, a number of composites have been studied and produced including Mg/Fe, Zn/Fe, Mg/Cu and Zn/Cu to accomplish the degradation of H_2O_2 to $^{\bullet}OH$ (Liu, Fan, & Wang, 2018)(Yang et al., 2019). Amongst the ZVMs, zero-valent iron (ZVI, Fe^0) is attractive because of its abundant availability and safety (Liu & Wang, 2019). As zero-valent iron is introduced to the reaction chamber containing dissolved O_2, it oxidizes to ferrous ion and releases two electrons facilitating the two-electron reduction of O_2 to H_2O_2, as it is precondition for the Fenton reaction. The dissolved O_2 then further reacts with H_2O_2 with Fe^{2+} as a catalyst to produce $^{\bullet}OH$ as shown by equations (1), (2) and (3).

$$\text{“}Fe^0 \rightarrow 2e^- + Fe^{2+} \qquad (E^\theta = -0{\cdot}44\ V)\text{”} \qquad \textbf{(2)}$$

$$\text{“}O_2 + 2H^+ + 2e^- \rightarrow H_2O_2 \qquad (E^\theta = 0{\cdot}695\ V)\text{”} \qquad \textbf{(3)}$$

$$\text{“}Fe^{2+} + H_2O_2 \rightarrow Fe^{3+} + {}^{\bullet}OH + OH^{-} \quad (k = 76\ M^{-1}\ s^{-1})\text{”} \qquad \textbf{(1)}$$

Many types of zero-valent metals, such as zero-valent zinc (Zn°) (Liu, Fan, & Wang, 2018), magnesium (Mg°) (Yang et al., 2019), aluminum (Al°) (H. Zhang et al., 2012) iron (Fe°) (Yang, Gong, Peng, et al., 2018) and copper (Cu°) (Long et al., 2020), have been employed for activation of O_2 to produce H_2O_2 to remove refractory organic pollutants by Fenton or Fenton-like process. Although, when zero-valent metal is used alone to activate O_2 to produce H_2O_2, the ZVM efficacy is very low. This is because the O_2 needs a substrate material to be transferred from bulk solution to accomplish reduction of O_2 and subsequent production of two electrons (Chen et al., 2020).

Fenton and Fenton-like processes require catalyst to mineralize the refractory organic contaminants. Although it is difficult to decompose H_2O_2 using iron-based catalysts to produce the ROS at neutral pH. Cu(I) has shown the ability to decompose H_2O_2 to OH over a wide pH range. Equation (4) shows that copper exists as Cu(II) under neutral pH conditions. (Wen et al., 2014) (Y. Zhang et al., 2017)

$$\text{“}Cu(I) + H_2O_2 \rightarrow {}^{\bullet}OH + Cu(II)\ (k_1 = 4 \times 10^5\ M^{-1}s^{-1} \text{ at pH 6–8)”} \qquad \textbf{(4)}$$

$$\text{“}H_2O_2 + Cu(II) \rightarrow Cu(I) + O_2^{\bullet-}\ (k_2 = < 1\ M^{-1}s^{-1} \text{ at pH 7)”} \qquad \textbf{(5)}$$

However, when H_2O_2 is decomposed to reactive oxygen species by Cu(I), copper ions will be released into the aqueous solution. Additionally, maintaining effective utilization of Cu(I) in Fenton-like process is difficult as Cu(I) rapidly oxidizes to Cu(II), that doesn’t have high catalytic activity for reduction of H_2O_2 to ROS (Long et al., 2020).

Studies have discussed various solutions to increase the rate of reduction of Cu(II) back to Cu(I) during the Fenton-like reaction. Regarding processes using Cu for activation of O_2, reductants like ZVI, Fe^{2+} and hydroxylamine could effectively reduce Cu(II) back to Cu(I) and facilitate degrading organic pollutants (Liu et al., 2020). Moreover, halide ions like F^- and Cl^- could also effectively reduce Cu(II) back to Cu(I) by forming CuF or CuCl (Gu et al., 2019).

Amongst these options the most efficient option would be addition of active metals like ZVI (Fe^0) as the products resulting from reduction of Cu(II) would be solid-state Cu^0 and Cu_2O which would decrease the amount of copper ions being released into effluent. Hence, it can be concluded that AC-Fe-Cu composite would be an effective Fenton-like catalyst that will not just achieve in-situ generation of H_2O_2 by activation of O_2 but also reduce H_2O_2 further into ROS at a broad pH due to presence of copper. Moreover, use of iron will decrease the amount of copper ions released into the effluent

1.3 Activated Carbon

As discussed earlier, the generation of hydrogen peroxide as a result of activation of oxygen just by a zero-valent metal is low due to the slow mass transfer of oxygen. According to the theory of electrochemical corrosion, this redox reaction occurs on metal surface forming numerous galvanic type corrosion cells in absence of external supply of power (Liu, Fan, Liu, et al., 2018). Hence, notable efforts have been dedicated to immobilizing zero-valent metals onto different carbon-based matrix materials, such as silica, activated carbon and carbon nanotubes to enhance the efficacy of oxygen activation. In this study, activated carbon is used as a substrate because of its high electrical conductivity and large surface area (which enhances the reaction rate) and low cost. Activated carbon enhances the reduction of oxygen to produce two electrons for generation of

ROS and augments the oxygen transfer from bulk to surface of activated carbon as it possesses high surface area and high porosity (Chen et al., 2020).

1.4 Methylene Blue

In this study Methylene Blue was selected as model compound for dyes. Methylene is widely used in textile industries. It is a water-soluble organic dye and it is injurious to human and animal health in way that it can cause eye burns which sometimes leads to permanent eye damage. Methylene Blue has other impacts on health as well including nausea, vomiting, diarrhea, breathlessness and mental confusion. Accordingly, effective mineralization of Methylene Blue has attracted notable attention in the environmental arena.

Advanced oxidation processes (AOPs) are extremely efficient to treat dyes such as Methylene Blue. These processes use reactive oxidation species (ROS) like hydroxyl radicals ($^{\bullet}OH$) for oxidation of organic contaminants.

1.5 Study Objectives

Objectives of this study were to:

- Synthesize AC-Fe-Cu composite at different temperatures and ratios to find the most effective composite for treatment of MB
- Evaluation of Methylene Blue degradation efficiency in AC-Fe-Cu/O_2 system using batch experiments.

2 Literature Review

2.1 In-situ generation of H_2O_2 in Zn-Fe-CNTs system for Fenton-like degradation of sulfamethoxazole (SMX)

Lui and his co-workers developed a novel Fenton-like Zn-Fe-CNTs catalysts which was employed for mineralization of sulfamethoxazole (SMX) using H_2O_2 as an oxidizing agent in a Fenton-like system. The composite was characterized using different characterization techniques including BET, EDS, SEM, TEM, XRD and XPS. Degradation efficiency of the composite was determined by varying initial concentration of SMX, initial pH and dosage of the composite. The method used for synthesis of this composite was infiltration fusion method followed by chemical replacement of iron on Zn-CNTs. The catalyst uses molecular oxygen to reduce it to H_2O_2 which is further reduced to $^{\bullet}OH$.

In this Zn-Fe-CNTs/O_2 system carbon (CNTs) acted as a cathode and Zn^0 acted as anode, releasing electrons after oxidizing. These electrons travelled to the cathode (CNTs) where two electron reduction of O_2 took place, reducing the O_2 to H_2O_2. Then Fe^0 catalyzed further reduction of H_2O_2 to $^{\bullet}OH$. This is called the Fenton-like process as Fe^0 is used to catalyze the reaction. This oxidation-reduction reaction occurs on metal surface forming numerous galvanic-type corrosion cells in absence of external supply of power. This phenomenon is called internal micro electrolysis.

The composite synthesized under this study efficiently removed SMX using Fenton-like degradation. According to the characterization techniques employed, the composite had coral structure with pores and exhibited a surface area of 51.67 m^2/g, demonstrating a high degradation efficiency for the pollutant, thus facilitating efficient removal of the pollutant. The composite was characterized after removal as well to confirm the presence of zinc and iron on composite. The composite gave a maximum removal efficiency of 100% under the following initial conditions:

- Initial pH of solution = 1.5,
- Initial solution temperature = 25ºC,
- Oxygen gas flow rate = 400 mL/min,
- Initial composite dosage = 0.6 g/L,
- Initial pollutant concentration = 25 mg/L
- Time = 10 min(Liu, Fan, & Wang, 2018)

2.2 In-situ generation of H_2O_2 for Fenton-like degradation of Sulfamerazine (SMR) using Al^0-CNTs and Fe-Cu-CNTs at neutral pH

Active metals are used for activation of O_2 due to a number of advantages like simple operating conditions and no external power requirement. However, O_2 is not very soluble in water decreasing its mass transfer efficiency and hence resulting in low degradation efficiency of contaminants. Moreover, when a single active metal is used its ability to reduce O_2 further to H_2O_2 is not sufficient. Thus, many matrix materials like graphene, cellulose, silica, carbon nanotubes, and activated carbon can be used for enhancing the efficiency of O_2 activation. Many zero-valent metals with high reduction potential like zero-valent iron, aluminum, zinc, magnesium etc. can be used to synthesize composites with CNTs for higher H_2O_2 generation efficiency. H_2O_2 has an oxidation potential of 1.78 V, which is relatively low. Hence, to accelerate oxidation capacity of the system, H_2O_2 can be reduced to $^{\bullet}OH$ which has an oxidation potential of 2.8V. Iron and its compounds are a good choice for catalytic decomposition of H_2O_2 as they have a high $^{\bullet}OH$

generation rate. However, mono-metallic iron-based catalysts do not degrade pollutants effectively under neutral pH conditions since iron is active over a very narrow pH range (2-3)

Therefore, in this study, carbon nanotubes were used as the matrix material as they possess very large surface area and high electrical conductivity. These composites are used as heterogeneous catalyst as they have optimum performance at neutral solution pH. The synthesis process of composite involved reduction followed by a displacement reaction. The composite was characterized using SEM, EDS, XRD and BET. In-situ H_2O_2 was being generated by Al^0-CNTs under oxygen supply. The generated H_2O_2 were reduced to $^{\bullet}OH$ by the Fe-Cu-CNTs composite. The advantage of this catalytic system was that degradation of SMR was being achieved over a broad range of pH. The composite gave a maximum removal efficiency of 85% at following conditions:

- Initial solution pH = 5.8,
- Initial solution temperature = 25ºC,
- Oxygen gas flow rate = 400 mL/min,
- Initial composite dosage = 1 g/L,
- Initial pollutant concentration = 50 mg/L
- Time = 60 min (Chen et al., 2020)

2.3 Fenton like Degradation of Sulfamerazine (SMR) at wide pH using Al^0-CNTs-Cu_2O composite for activation of O_2 to H_2O_2

Fenton-like processes require a catalyst for oxidation of the organic pollutants. But efficiency of Fe based catalysts is low at neutral pH for conversion of H_2O_2 to reactive oxygen species. This study demonstrates that Cu^+ can reduce H_2O_2 to $^\bullet OH$ over a wide range of pH as shown in equation 4.

$$\text{“}Cu(I) + H_2O_2 \rightarrow {}^\bullet OH + Cu(II) \qquad (k_1 = 4\times10^5\ M^{-1}\ s^{-1} \text{ at pH 6–8)”} \qquad \textbf{(4)}$$

At neutral pH conditions, Cu^{2+} predominantly exists as $[Cu(H_2O)_6{}^{2+}]$. However, when Cu^+ will catalyze the reduction of H_2O_2, copper ions will be released in the aqueous solution. Also, Cu^+ rapidly oxidizes to Cu^{2+}, inhibiting the reduction of H_2O_2 as Cu^{2+} does not have high reduction potential at neutral pH. (equation 5)

$$\text{“}H_2O_2 + Cu(II) \rightarrow Cu(I) + {}^\bullet O_2^- \qquad (k_2 = < 1M^{-1}\ s^{-1} \text{ at pH 7)”} \qquad \textbf{(5)}$$

Liu et al. synthesized a novel Al^0-CNTs-Cu_2O Fenton-like catalyst which efficiently reduced O_2 to H_2O_2 and subsequently reduced H_2O_2 to ROS over a broad pH for removal of SMR. The synthesized composite was characterized using BET, EDS, SEM, XRD, XPS and FT-IR. The catalyst was then used for degradation and removal of SMR from wastewater. H_2O_2 were produced by the reduction O_2 using the composite.

This H_2O_2 was then reduced to $^\bullet OH$ and $^\bullet O_2$ by Cu^+, producing Cu^{2+} which can be reduced back to Cu^+ by the Al^0 in Al^0-CNTs composite. Due to reduction of Cu^{2+} back to Cu^+, the process becomes more efficient and sustainable as Al^0-CNTs composite could be reused while decreasing the release of copper ions in the solution.

The composite gave a removal efficiency of 73.91% of SMR under the following initial conditions:

- Initial solution pH = 5.8,
- Initial solution temperature = 20ºC,

- Oxygen gas flow rate = 100 mL/min,
- Initial composite dosage = 2 g/L,
- Initial pollutant concentration = 50 mg/L
- Time = 60 min

Copper ion concentration in the reaction chamber was also determined which was less than 0.5 mg/L. The prepared composite could efficiently generate in-situ H_2O_2 using Fenton-like process, for mineralization of organic contaminants over broad pH range (Liu et al., 2020).

2.4 In-situ generation of H_2O_2 for catalytic wet peroxidation of high concentration 4-Chlorophenol by Zn-CNTs-Cu composite

Novel Fenton-like Zn-CNTs-Cu catalyst was synthesized for removal 4-Chlorophenol (4-CP) in high concentration using a catalytic wet peroxidation system (CWPO) as high concentrations of 4-CP are difficult to remove through traditional methods. High 4-CP concentration is difficult to remove using traditional treatment technologies, such as membrane processes, coagulation, flocculation etc., because it has high biotoxicity and its resistance to bio-degradation. For this reason, Fu et al., developed a novel CWPO system for oxidation of high 4-CP concentration using in-situ generated H_2O_2 by Zn-CNTs-CU catalyst. Under this study, operating factors, mechanism of degradation and degradation pathways of 4-CP were evaluated and reported. Zn-CNTs-Cu composite employed with CWPO resulted in obtaining 100% degradation of 4-CP, which was 689 % more than that of CWPO-O_2 system alone.

Because of the synergetic effect of highly oxidative hydroxyl radical and CWPO effect of O_2, the Zn-CNTs-Cu catalyst degraded high amount of 4-CP to smaller chained compounds, carbon dioxide and water. In conclusion, the Zn-CNTs-Cu composite with CWPO along with O_2 effectively degraded the high amountof 4-CP using Fenton-like Process. This is an innovative method for mineralization of organic pollutants like chlorophenols (Fu et al., 2021).

2.5 Fenton-like oxidation of 4-chlorophenol using H_2O_2 in situ generated by Zn-CNTs-Fe composite

Liu and his group also studied the removal of 4-chlorophenol (4-CP) using a Zn-CNTs-Fe composite. The composite was synthesized using infiltration-fusion method, which resulted in the formation of Zn-CNTs followed by chemical precipitation of iron using $FeSO_4.7H_2O$ Zn-CNTs. The composite was then characterized using TEM, BET, XRD and XPS. Then the composite was used to evaluate the degradation efficiency of the 4-CP using a Fenton-like Zn-CNTs-Fe/O_2 system which produced in-situ H_2O_2. When zinc and carbon contacted with water they formed numerous galvanic cells, without any external power source, and internal micro-electrolysis took place between zinc and carbon to produce H_2O_2 using O_2. The H_2O_2 produced was further reduced to $^{\bullet}OH$ by iron. Both H_2O_2 and $^{\bullet}OH$ degraded 4-CP into smaller chain organic compounds, carbon dioxide and water. To determine the amount of H_2O_2 produced during the reaction, a UV-vis spectrophotometer was employed at wavelength of 385 nm. Characterization techniques reveled that the zinc and iron particles were bonded to the surface of carbon nanotubes, enhancing the transfer of electrons from oxygen to the solution. Composite surface area was $32.9 m^2/g$ and percentage composition by weight of Zn was 44.7% and that of iron 4.2%. The composite gave a maximum removal efficiency of 90.8% under the following initial conditions:

- Initial solution pH = 2.0,

- Initial solution temperature = 25ºC,
- Oxygen gas flow rate = 800 mL/min,
- Initial Composite Dosage = 1.0 g/L,
- Initial Pollutant Concentration = 50 mg/L
- Time = 20 min (Liu, Fan, Liu, et al., 2018).

2.6 In-situ synthesis of hydrogen peroxide in a novel Zn-CNTs-O_2 system

A novel method was formulated and investigated to produce in-situ generation of H_2O_2. Molecular oxygen formed H_2O_2 along with production of Zn^{2+} in the CNTs-Zn system. Following parameters were studies to enhance in-situ H_2O_2 production;

1. Mass ratio of zinc and CNTs
2. Synthesis temperature
3. Composite dosage
4. Initial solution pH
5. Temperature of the system
6. Oxygen gas flowrate

Maximum H_2O_2 accumulation, 293.51 mg L^{-1}, was shown within 60 minutes when Zn-CNTs mass ratio was 2.5:1, synthesized at 500 degree Celsius, initial pH was 3.0, Zn-CNTs dosage was 0.4 g and oxygen gas flow rate was 400 mL min^{-1}. O_2 produced H_2O_2 on CNTs through two-electron pathway whereas, the Zn^0 was oxidized to Zn^{2+} in the system and the oxidized Zn^{2+} ions formed zinc hydroxide which accumulated on CNTs surface. This process is a reliable strategy for the in-situ generation of H_2O_2 as it is environmentally friendly and economical (Gong et al., 2018).

2.7 Generation of hydroxyl radicals from reactions between a dimethoxyhydroquinone and iron oxide nanoparticles

•OH is an efficient oxidant which can be produced using the Fenton reaction in different environments. The reactants are generated as Fe^{3+} and O_2 are reduced. This reduction can be encouraged by organic reducers like hydroquinones. This study investigated amount of hydroxyl radical generated as a result of reaction of 2,6-dimethoxyhydroquinone (2,6- DMHQ) with nano-sized iron oxide. Reactiveness of ferrihydrite and goethite were also compared and to study the impact of pH and O_2 on production of ·OH. The study revealed that reaction of nano-sized iron oxide and 2,6-DMHQ produced considerable quantity of ·OH, through the redox reactions, while a particular environment was maintained. To accomplish production of H_2O_2 and to catalytically degrade 2,6-DMHQ, it was necessary to provide oxidative environment. Furthermore, ease of reduction of ferrihydrite as compared to goethite made ferrihydrite more prone to dissolution by reduction, enhancing the generation of ·OH (Lyngsie et al., 2018).

2.8 Fenton degradation of 4-chlorophenol (4-CP) using H_2O_2 in situ generated by Zn-CNTs/O_2 system

For purpose of this study the infiltration fusion method was used to synthesize Zn-CNT composites and the composites were characterized using BET, TEM and XPS. Zn-CNTs and O_2 were reacted along with solution of the pollutant for the in-situ generation of H_2O_2, which then reacted with Fe^{2+} to accomplish Fenton-like degradation of 4-CP. The effects of different factors like composite loading, pH, and ferrous ion concentration were investigated for the removal of 4-CP. Composite gave treatment efficiency of 98.8% under the following conditions;

- Initial solution pH = 2.0,

- Oxygen gas flow rate = 400 mL/min,
- Initial composite dosage = 2.0 g/L,
- Ferrous ion concentration: 20mg L-1
- Time = 20 min

Under the above-mentioned conditions, the treatment efficiency of 4-CP was reduced to 47.0% as 4-CP concentration elevated in the secondary effluent of a wastewater treatment plant. To study intermediates, LC-MS and IC were employed to suggest the likely route by which the mineralization of 4-CP took place (Liu et al., 2017)

2.9 Zn^0-CNTs-Fe_3O_4 catalytic in situ generation of H2O2 for heterogeneous Fenton degradation of 4-chlorophenol

A novel Fenton-like Zn^0-CNTs-Fe_3O_4 composite was prepared in nitrogen atmosphere by employing chemical co-precipitation and high temperature sintering. The synthesized composite was analyzed using BET, EDS, SEM, XRD, VSM, XPS. A novel Fenton-like system was created, which was heterogenous in nature, to generate in-situ H_2O_2 using the composite and dissolved oxygen from the solution. The generated H_2O_2 is oxidized to $^{\bullet}OH$ by the system for mineralization of 4 chlorophenol

The effect of different operating factors like composite dosage, pollutant concentration, and pH were studied for mineralization of 4-CP. The composite gave a maximum removal efficiency of 99% under the following initial conditions:

- Initial solution pH = 1.5,
- Initial solution temperature = 25ºC,
- Initial composite dosage = 2.0 g/L,

- Initial pollutant concentration = 50 mg/L

The radical scavenger effect study revealed that the hydroxyl radical was primary oxidizing agent for mineralization of 4-CP (Liu et al., 2017).

2.10 A novel carbon nanotube–magnesium oxide composite with excellent recyclability to efficiently activate peroxymonosulfate for Rhodamine B degradation

It is the need of the hour to develop an environmentally friendly way for treating organic contaminants in wastewater. In such a way, Rhodamine B (RhB) can be degraded by activation of peroxymonosulfate using carbon nanotube-magnesium oxide composite (CNTs/MgO). The characterization techniques used for characterization of synthesized CNTs/MgO were BET, SEM, TEM, FTIR, XRD and XPS. It was observed that the carbon nanotubes formed a uniform network on surface of MgO connecting to MgO by C-O and Mg-C bonds. The treatment efficiency of the synthesized CNTs/MgO was determined by the studying the effect of parameters such as pH, ratio of MgO/CNTs, CNTs/MgO dosage, peroxymonosulfate dosage and temperature on removal of RhB. The removal experiments were performed at broad pH (3-9). 100% RhB was removed in 20 mins under optimal environment. Furthermore, effective removal was achieved due to the oxygen in the lowest excited state, which was produced in the PMS & CNTs/MgO system. The reason for enhanced activation of CNTs/MgO was the accelerated electron transfer and the bond strength of CNTs and MgO. The works is also very helpful in providing an advanced process to produce innovative peroxymonosulfate catalysts without using of transition metal compound (Peng et al., 2020)

2.11 In situ generation of H_2O_2 using MWCNT-Al/O_2 system

Hydrogen peroxide, being environmentally friendly oxidizing agent, has been largely employed for AOPs to accomplish removal of harmful organic pollutants. Because of high transportation cost and safety issues associated with storage of H_2O_2, in-situ H_2O_2 generation is a feasible option as the capital and operation costs would be reduced. For purpose of this research study, a unique composite of multi-walled carbon nanotube and aluminum (MWCNT-Al) was synthesized, characterized and optimized. The composite was capable of generating in-situ H_2O_2 via micro electrolysis. 947 mg/L of H_2O_2 accumulated in the system at the following initial conditions:

- Initial solution pH = 9.0,
- Composite dosage = 8 g/L
- Oxygen gas flowrate = 400mL/min
- Time = 60 min

In-situ H_2O_2 generation of the MWCNT-Al catalyst along with oxygen gas was because of the interaction of MWCNT and Al^0 as it improved the electron transport from aluminum to oxygen. This led to the release of two electrons from oxygen, facilitated due to the excellent electrocatalytic activity of MWCNT (Tan et al., 2019).

2.12 Efficient in situ generation of H_2O_2 by novel magnesium–carbon nanotube composites

Yang and his co-workers developed an innovative magnesium-carbon nanotube (Mg-CNT) catalyst by employing ball milling process under inert environment. Polyvinylidene fluoride (PVDF) was used to bind the CNTs with magnesium. The synthesized catalyst was capable of generating in-situ H_2O_2. The composite was then optimized by analyzing the effect of different operating parameters and synthesis conditions, thus improving the efficiency of in-situ H_2O_2 generation. The maximum concentration of in-situ generated H_2O_2 produced using the Mg-CNT composite was 194.73 mg/L under following conditions:

- Contact time with oxygen gas = 60 min
- Mass ratio of Mg:CNT:PVDF = 5:1:2.4

Mg-CNT composite used the dissolved oxygen in the solution to reduce it to H_2O_2 whereas Mg was oxidized releasing two electrons. These electrons facilitated the reduction of O_2 to generate two electrons for subsequent production of H_2O_2. Some of Mg^{2+} ions formed $Mg(OH)_2$ and precipitated onto carbon nanotubes. Moreover, study suggested that the micro-electrolysis taking place on Mg-CNT catalyst due to formation of galvanic type corrosion cells promoted the generation of in-situ H_2O_2. Using this composite for mineralization of toxic organic contaminants in wastewater is an environmentally friendly approach as it uses a strong oxidizing agent (H_2O_2) which is generated in-situ (Yang, Gong, Wang, et al., 2018).

3 Experimental Work

This chapter encompasses the experimental details, chemicals used for the synthesis of composites, various techniques used for the characterization of synthesized composites and the procedure opted to mineralize Methylene Blue. Synthesis of AC-Fe-Cu composite has been discussed in detail. Photocatalytic degradation of Congo red and its mechanism has been discussed in detail

3.1 Materials and Methods

3.1.1 Chemicals and reagents

The chemicals and reagents employed in the research were all from Sigma Aldrich which were of analytical grade and commercially available. They were not purified further and were used as received. List of the chemicals used has been provided in Table 3.1

Table 3.1: Chemicals used for the study

Chemical	**Supplier**
Activated Carbon	Sigma Aldrich
Iron metal powder	Sigma Aldrich
Copper metal powder	Sigma Aldrich
Polyethylene glycol (PEG) 4000	Sigma Aldrich
Argon gas	Sigma Aldrich
Methylene Blue	Sigma Aldrich
DI water	Sigma Aldrich
Sulfuric acid	Sigma Aldrich

Sodium hydroxide	Sigma Aldrich
Potassium titanium oxalate	Sigma Aldrich
Potassium permanganate	Sigma Aldrich
Hydrogen peroxide	Sigma Aldrich

3.1.2 Synthesis of AC-Fe-Cu Composites

AC-Fe-Cu composites were synthesized at different mass ratios and different temperatures to study the effect of heat treatment and varying ratio on treatment of MB. The ratio of activated carbon and iron was kept constant at AC:Fe – 3:1. The ratio of Cu was varied to study the effect of generation of H_2O_2 and its subsequent reduction to $OH^{\bullet}$ on treatment of MB. The composite was first synthesized at 300, 500 and 700 degree Celsius while keeping the ratio of composite constant i.e.; AC:Fe:Cu – 3:1:1. Then treatment efficiency of the composite at these three temperatures was tested. Based on the characterization results and treatment efficiency, the temperature at which the composite gave the highest percentage removal was and further composites were synthesized at that temperature while varying the ratio of Cu. The detail of the ratios and mass is presented in Table 3.2

Table 3.2: Detail of composite ratios and mass

Composite Ratio	Total Mass (g)	Mass of Activated Carbon (g)	Mass of Iron (g)	Mass of Copper (g)
AC:Fe:Cu – 3:1:2	10	5.00	1.67	3.33
AC:Fe:Cu – 3:1:1	10	6.00	2.00	2.00

AC:Fe:Cu – 3:1:0.5	10	6.67	2.22	1.11
AC:Fe:Cu – 3:1:0.25	10	7.06	2.35	0.59
AC:Fe:Cu – 3:1:0.125	10	7.27	2.43	0.30
AC:Fe:Cu – 3:1:0	10	7.5	2.5	0

To synthesize AC:Fe:Cu composite, respective mass of activated carbon, iron metal powder and copper metal powder was weighed using an analytical balance and transferred to a china dish. Initial mass of oven dried china dish was weighed using an analytical balance. The mass of china dish with the dry contents i.e.; activated carbon, iron metal powder and copper metal powder was also measured. The dry contents were mixed thoroughly using a spatula. Then 5ml of 40% w/v polyethylene glycol 4000 solution was added into the dry mixture and stirred thoroughly with a spatula until uniformly mixed. Mass of china dish, dry contents and PEG 4000 was also measured. This mixture was then kept in a tube furnace, while ensuring minimum contact with air to avoid oxidation. Argon (Ar) gas was purged from the tube furnace at 100 ml/min flow rate for 20 minutes. The mixture was then sintered in the tube furnace at 300, 500 and 700 degrees Celsius for 2 hours at an Ar flow of 60 ml/min. After 2 hours of sintering, Ar gas was again purged from the tube furnace the same initial flow rate for 20 mins. The composite was removed as the reactor cooled to room temperature, again ensuring minimum contact with air. Mass of china dish + composite was measured to calculate the loss in mass. The detail of measured mass of china dish, china dish + dry contents, china dish + dry contents + PEG and china dish + composite is shown in Table 3.3

Table 3.3: Detail of mass of components

Mass of components	Composite Ratio (AC:Fe:Cu)							
	3:1:2	3:1:1			3:1:0.5	3:1:0.25	3:1:0.125	3:1:0
	500ºC	300ºC	500ºC	700ºC	500ºC	500ºC	500ºC	500ºC
China dish (g)	26.12	26.79	25.93	24.87	25.93	23.98	23.99	25.59
China dish + dry contents (g)	36.20	36.83	35.7	34.82	35.91	34.1	33.75	35.59
China dish + dry contents + PEG (g)	41.50	41.6	40.1	39.95	40.3	39.6	39.03	40.9
China dish + composite (after sintering) (g)	35.91	35.93	35.16	34.56	35.16	33.8	33.34	35.34
Weight of composite (g)	9.79	9.14	9.23	9.69	9.23	9.82	9.35	9.75

In this process, PEG 4000 was used as a binder to bind activated carbon, iron and copper and to ensure uniform distribution of iron and copper on activated carbon. PEG 4000 decomposed into volatile gases as its boiling point is 200ºC.

3.1.3 Degradation of MB via AC-Fe-Cu composite

Batch degradation experiments for MB were conducted in a 100 ml glass beaker. The concentration of MB was 50 mg/L, composite dosage was 1 g/L, initial solution pH was 4, reaction time was 2 hours and reaction volume was 50 ml. All the experimental work was done at room temperature. Solution pH was maintained using H_2SO_4 (0.1mol/L) and NaOH (0.1mol/L). For preventing any interference related to pH change, the solutions were not buffered. An aerator and a diffuser were used to provide air (for oxygen) at the bottom of the reaction chamber. When the AC-Fe-Cu composite, O_2 and water all came in contact, many galvanic-type corrosion cells were generated in the solution.

During treatment, 5 mL samples were drawn at 30 minutes interval and filtered using a 0.22µm membrane before analysis. These samples were withdrawn to analyze the residual concentration of MB and the concentration of H_2O_2 generated during the reaction. Then absorbance of the filtered sample was measured at 655 nm to determine the concentration of MB remaining in the sample by employing a UV-Vis Spectrophotometer. Concentration of H_2O_2 generated was determined at 400 nm by employing a UV-Vis Spectrophotometer. The experimental work was performed in duplicated, and the results of those experiments were presented as mean value. The absorbance of samples was also measures in duplicates and mean values were expressed.

3.2 Characterization Techniques

The confirmation of the as-synthesized product was done using different characterization techniques. To confirm the composition of elements of the composites, EDS analysis was carried out along with elemental mapping. SEM was employed to study the surface characteristics of the composites using a Hitachi S4800 field emission scanning electron microscopy (FESEM) with energy dispersive X-ray spectroscopy (EDS). The acceleration voltage had been set at 20kV. This analysis was performed at School of Chemical and Materials Engineering (SCME), NUST. Crystal structure of the product was probed using XRD analysis. A Rigaku diffractometer with Cu-Kα radiation equipped with graphite monochromator was used for the analysis of crystal structure. XRD patterns were analyzed over a 2θ range i.e. $0^{o} – 120^{o}$ with a time count of 1 second.

These analyses were performed at Pakistan Institute of Engineering and Applied Sciences (PIEAS). Textural Properties of composites were determined by adsorption-desorption isotherms at nitrogen temperature 77K by using surface area and pore size analyzer. All the samples were degassed for 3 hours at 120^{o}C. These analyses were performed at department of chemistry and chemical engineering at LUMS, Lahore. Instrumentation and working principle of different characterization techniques has been discussed as below:

3.2.1 Energy Dispersive X-ray Spectroscopy (EDS)

EDS is an is employed for qualitative and quantitative analysis of a material. EDS determines the chemical makeup of the composite. It detects and analyzes elements with atomic number of 3 or more. Electromagnetic radiations strike with matter, and result in the emission of X-rays. Every element possesses a characteristic emission pattern because of its unique atomic structure. Atoms when at rest, are in the ground state. When a high energy beam of X-rays or electrons strike the sample, electron excites to a higher energy level, leaving behind a vacant electron position. Electron possessing higher energy occupies this vacant position. Electron releases the energy (in the form of X-rays) which is equal to the difference of energies between the two levels.

Energy dispersive spectrophotometer measures the released energy. Energy difference between two shells is characteristic of an element, hence in this way elemental composition of a material can be determined using energy dispersive spectrophotometer. Peak position helps in qualitative analysis of the sample, whereas peak height reflects to the concentration of a particular element. Characteristic X-rays of elements are separated by EDX detector into an energy spectrum. An EDX Spectra is a plot between X-ray counts and energy. As each element shows a distinct X-ray absorption pattern, therefore the identification of the elements and their concentration can be estimated by EDX analysis (“Physical Principles of Electron Microscopy,” 2005).

Major components of an energy dispersive spectrophotometer include:

- Source of radiation
- X-ray detector
- Pulse processor
- Analyzer

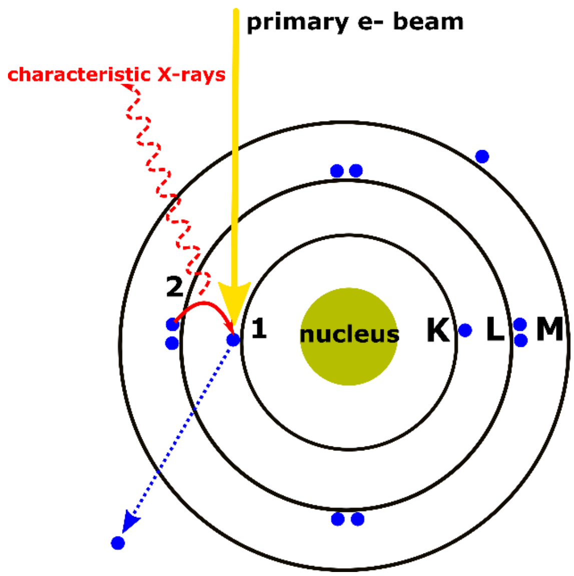

Figure 3.1: Mechanism of electron and characteristic X-ray emission resulting from electron irradiation

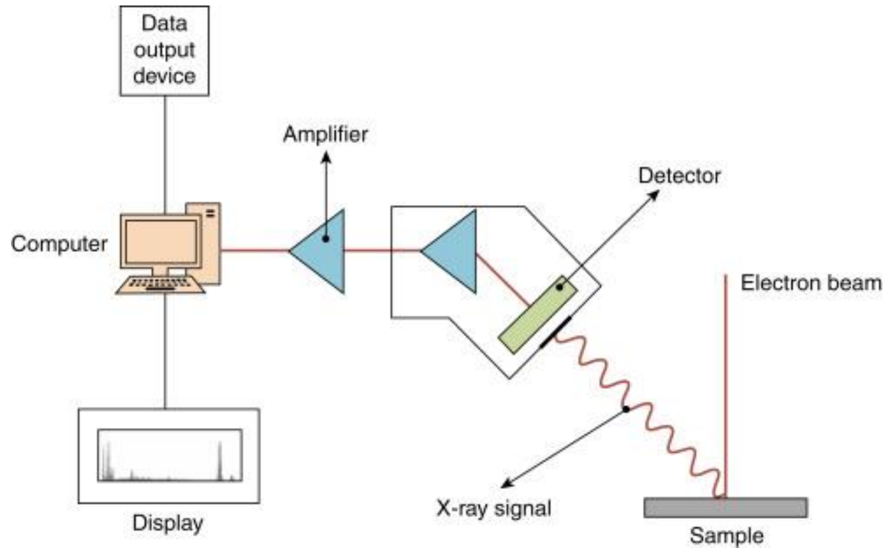

Figure 3.2: Working principle of Energy Dispersive X-ray Spectroscopy

3.2.2 Scanning Electron Microscopy (SEM)

The principle of SEM works by using high-energy beam of electron which is focused on the sample surface, creating an image. The electrons are incident on the sample and the get scattered after coming in contact with the specimen. They then lose the energy which gets absorbed. Range of the scattering is related to the atomic number and density of the elements of which the sample is composed of. The range of scattering is directly proportional to energy however it is inversely proportional to the atomic number and density of the elements. Through this process, an image is obtained. When incident beam of electron comes in contact with the specimen, it produces numerous signals. To determine the composition (SEM is used along with EDS) and surface characteristics of the sample, an area of the sample is selected and analyzed. The data collected is processed and a two-dimensional image is formed. This data can also be obtained for specific points for the specimen ("Physical Principles of Electron Microscopy," 2005).

Scanning electron microscope comprises of the following components:

- Electron probe
- Specimen stage
- Electromagnetic lens
- Secondary electron detector
- Image display unit
- Operation system

For electron source, an electron gun is used which is positioned at the top of the instrument. There are two types of guns that are used – thermionic gun and field emission gun. In order to obtain a higher magnification of the sample, larger number of electrons are used (James, 2003). The electrons are directed towards the specimen by an electromagnetic lens which is located in the vacuum chamber. When the incoming electron beam comes in contact with the sample, different types of electrons are emitted like backscattered electrons, auger electrons and secondary electrons. Different types of detectors detect these electron. Each type of emitted electron provides different information i.e., backscattered electrons are used for distinguishing different phases in multiphase samples whereas secondary electrons are used for the surface morphology ("Physical Principles of Electron Microscopy," 2005).

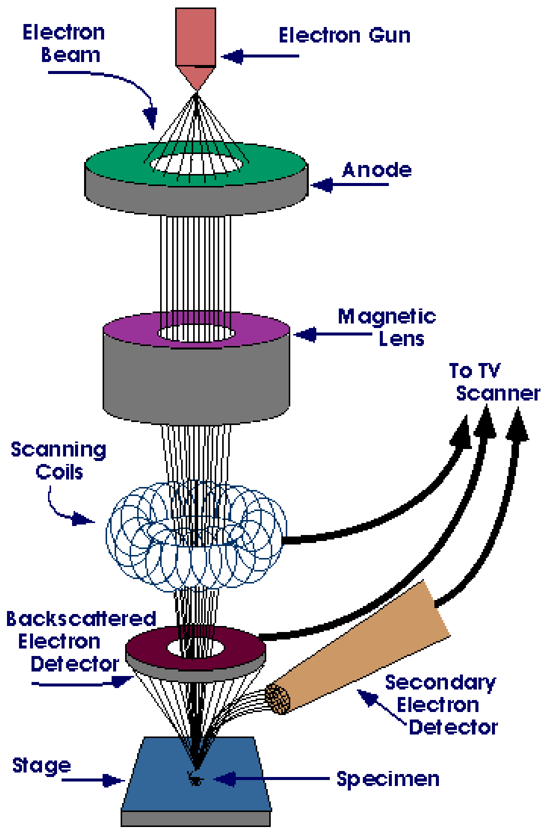

Figure 3.3: Working of a Scanning Electron Microscope

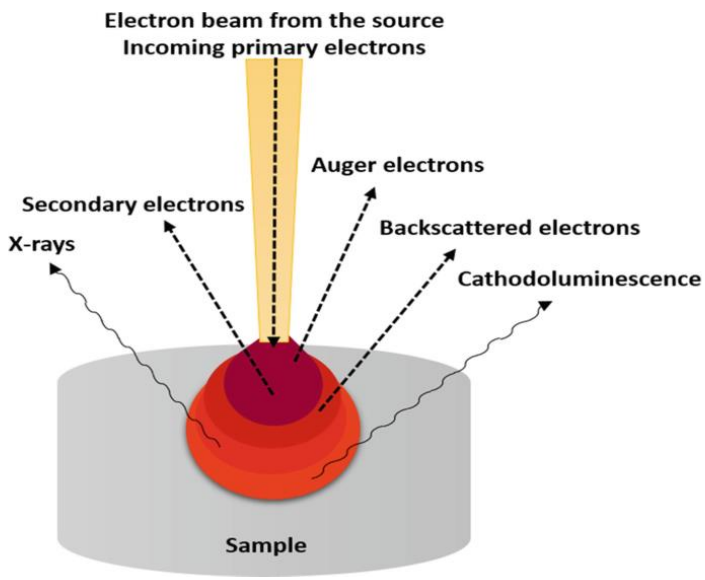

Figure 3.4: Interaction of electron beam with the sample in SEM

3.2.3 X-ray Diffraction (XRD)

XRD analysis determines the crystalline structure of a sample. It is a non-destructive technique which employs phase identification. A crystalline sample is comprised of different layers and planes. When the distance between atoms is same as the wavelength of the incident X-rays, diffraction takes place when incident angle is same as reflective angle. This phenomenon can be explained by using Bragg's Law which is:

$$\mathbf{2d\sin\theta = n\lambda}$$

Where:

- **d** = Distance between the planes,
- **θ** = diffraction angle
- **n** = integer,
- **λ** = wavelength of X-rays,

When reflection is being detected at the detector, constructive interference occurs which confirms that Braggs law is being satisfied. Interlayer spacing is determined by the position of the reflected ray. The amount of incident X-ray being reflected can be determined by the peak intensity. Parameters like crystallinity of the sample, crystal structure, density, cell volume, lattice parameters and phases present in the material can all be determined by the diffraction pattern of the sample (Tala-Tebue et al., 2016). Cathode emits electrons which then displace the electrons in the sample, which is mostly copper (Cu Kα = 0.54nm), generating an X-ray spectrum.

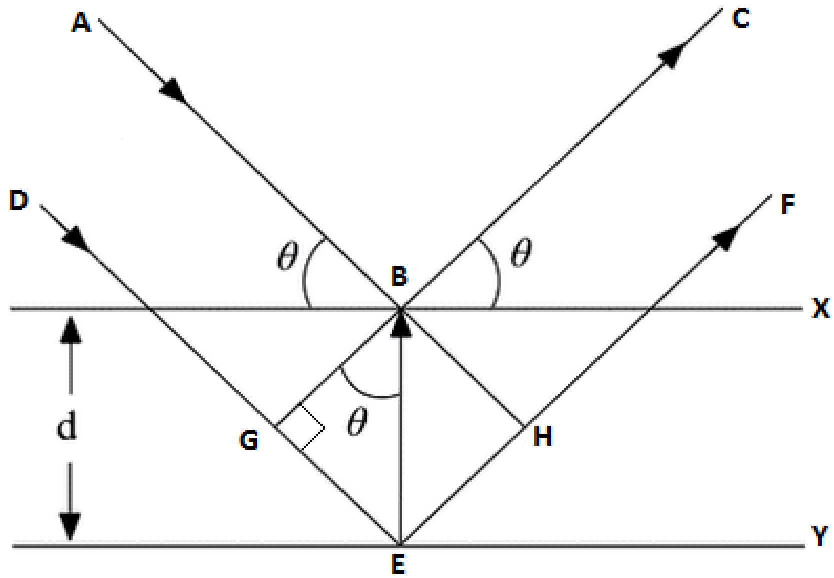

Figure 3.5: Illustration of Bragg's law

XRD comprises of:

- X-ray Source
- Monochromator
- Goniometer (It restricts the wavelength range)
- Sample holder
- Detector

An beam of X-rays is incident on a crystal which is then filtered by the Monochromator which then falls parallelly on the sample. The sample is then rotated within the path of X-rays at an angle equal to θ. The sample is rotated using a Goniometer. The diffracted x-rays are detected by the detector which revolves at an angle equal to 2θ. As the X-rays are diffracted and reflected back from the crystal layers, constructive interference occurs after which a diffraction pattern is obtained which is recorded on a photographic film. (Vinila et al., 2014)

XRD can be used for a number of applications including:

- Phase identification of material
- Determination of crystal structure
- Determination of texture, grain size and composition of thin film

3.2.4 Brunauer, Emmett and Teller (BET)

BET evaluates the data for gas adsorption for determining surface area of the sample, the units of which are m^2/g. This methodology is broadly employed for majority of materials but is appropriate for samples possessing Type II or Type III isotherms. The BET theory is not suitable for other types of isotherms, so it should be used accordingly.

Before determining the surface area, the specimen should be prepared in a way to get rid of impurities which have bonded with the sample before degassing. This can be usually achieved by exposing the sample to high temperatures in a vacuum or inert gas environment. In order to get consistent results the process of degassing should be carefully conducted while monitoring the process. (Dollimore et al., 1976)

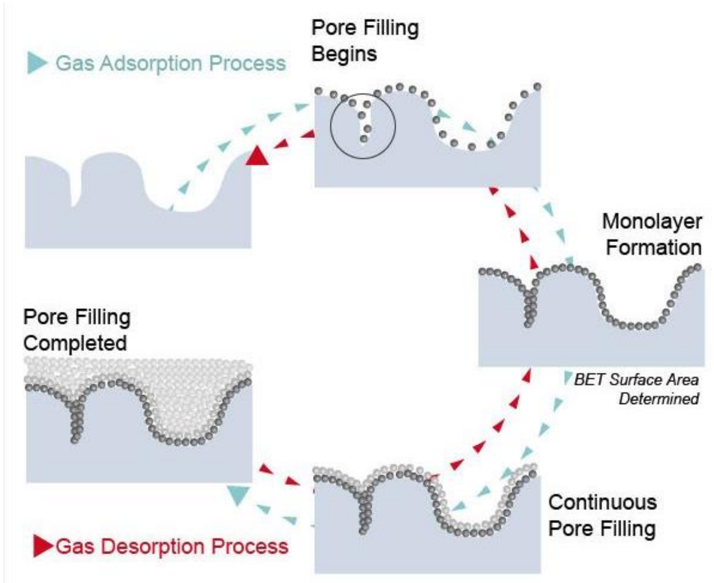

Figure 3.6: Gas adsorption-desorption process in BET analysis

3.3 Analytical Methods

To determine the concentration of MB and H_2O_2 generated during the reaction, UV–vis spectrophotometer was used. H_2O_2 concentration was determined using photometric method at a wavelength of 385 nm while employing potassium titanium oxalate as chromogenic reagent. Whereas MB was measured at 655nm. UV-Visible Spectrophotometer helped in collecting the UV-Vis diffuse reflectance pattern within a wavelength range of 200-800nm. A lambda 750 UV/Visible spectrophotometer with 200-800 wavelength range and was used for collecting UV-visible diffuse reflectance spectra. BaSO4 was used as a reference

3.3.1 UV-Vis Spectrophotometer

The analysis using a spectrophotometer is both quantitative and qualitative. A wavelength between 200-400nm corresponds to the ultraviolet band of the electromagnetic spectrum, while a wavelength between 400-800nm corresponds to visible light portion of electromagnetic spectrum. Spectrophotometer works according to the principle of absorbance, reflectance and transmittance.

Incident beam on the sample is of a specific wavelength. As it passes through the sample, some of it gets absorbed whereas some of it is reflected and transmitted to the detector called a photodetector. The photodetector then measures the energy of the radiations that were transmitted through the sample, thus giving the absorbance of the sample.

When the light gets absorbed by the sample at a specific wavelength, the electrons in the sample are excited. The absorbance is equal to the difference in energy between the newly occupied orbital and previously occupied orbital. This process occurs a number of times, giving an absorption spectrum. The absorbance is plotted against the corresponding wavelength, giving a UV-vis spectrum, while a plot of wavelength against reflectance gives a UV-diffuse spectrum. Spectrophotometer follows the principle of Beer-Lambert Law which explains the relation between the thickness of the solution and the absorbance of the sample. Solution absorbance increases as viscosity increases. This law is represented by the following equation:

$$\mathbf{A = E\ c\ L}$$

Where,

A = absorbance

E = absorptivity coefficient

c = solution concentration

l = path length

Transmittance is calculated by dividing transmitted light by incident light. Absorbance is inverse of transmittance.

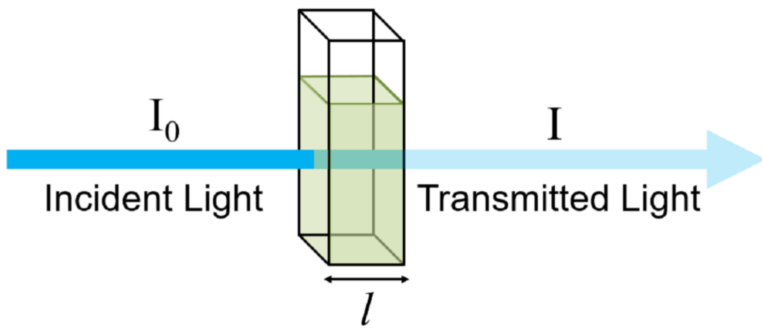

Figure 3.7: Beer-Lambert law

A UV-vis spectrophotometer consists of the following components:

- Light Source
- Monochromator
- Holder for the sample
- Detector
- Processor and a read-out device

There are two types of lamps used as source of light for the UV-vis spectrophotometer. One is used for providing UV radiation which is Hydrogen-deuterium lamp. Other is used for providing visible light source which is tungsten filament lamp. To reflect UV radiation on a monochromator, a solenoid mirror is employed. Monochromator consists of a number of components like prism, entrance slit, exit slit, mirrors. The purpose of the prism is to produce monochromatic light from polychromatic light. This monochromatic light passes through the exit slit and becomes incident on beam splitter. Once the light passes through the beam splitter, it gets split into two beams, one beam passes through the reference compartment and other passes through the sample. Both reference and sample absorb some of the light and absorbance of the sample is determined by calculating the difference between the light absorbed by the sample and the reference. A photodiode is also used to produce electrical signal. This signal is enhanced so that it can be detected by the read-out device. The absorption of the sample against corresponding wavelengths is recorded, producing a UV-vis spectrum. (*Alnatt Und A . B. Lidiard:*, 1995)

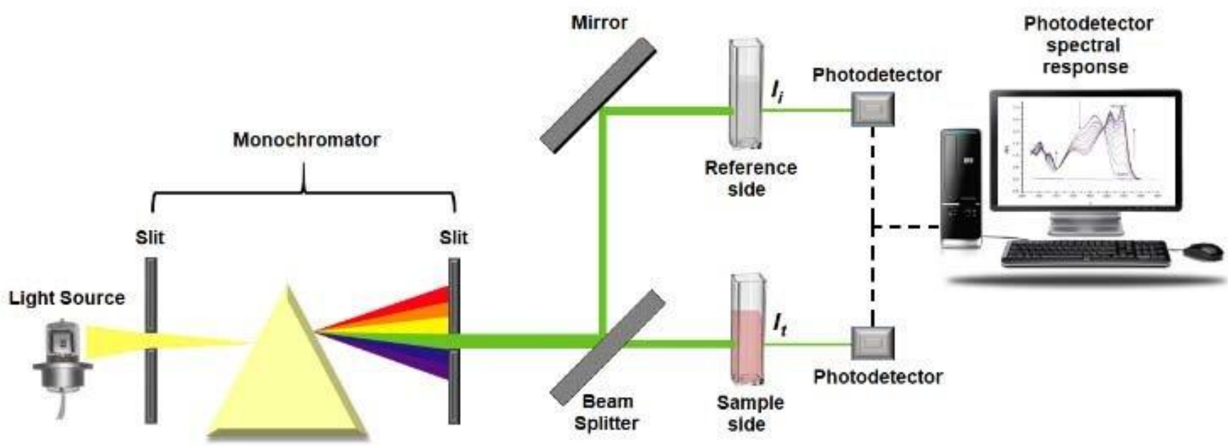

Figure 3.8: UV-Vis spectrophotometer

4 Results and Discussions

Following chapter encompasses results of degradation of Methylene Blue and characterization results of synthesized composites.AC-Fe-Cu composite was first synthesized at three different temperatures while keeping the mass ratio constant. Treatment efficiency of these three composites was evaluated and the temperature at which the composite was giving the highest removal was selected to vary the mass ratios of copper. The as-synthesized material was then characterized using different techniques, to confirm the surface area, elemental composition, morphology, and crystal structure.

Experimentation was conducted in three phases:

1) Synthesis of novel Fenton-like AC-Fe-Cu composites
2) Characterization of novel Fenton-like AC-Fe-Cu composites
3) Methylene Blue degradation experiments

4.1 Characterization Results

4.1.1 Energy Dispersive X-ray Spectroscopy (EDS)

To confirm elemental composition of composites, EDS was carried out. First of all activated carbon that was used to synthesize was analyzed by EDS to know the elemental composition of activated carbon. Figure 4.1 shows EDS graph of activated carbon which shows presence of carbon, oxygen, magnesium, aluminum, silicon, chlorine, calcium and iron in the activated carbon. The weight and atomic percentages of these elements are shown in the Table 4.1. The presence of oxygen indicates partial oxidation of sample during characterization. The graphs in Figure 4.2 to Figure 4.4 and data in Table 4.2 to Table 4.4 show the presence of carbon, iron and copper in the composites Cu-1 synthesized at 300, 500 and 700 degrees Celsius. Both iron and copper are present in the composites. Content of the copper in the composite increases with the increasing temperature of synthesis. The composite synthesized at 300 degree Celsius, has 0.07% of copper whereas at 500 degree Celsius it is 11.32% and at 700 degree Celsius it is 18.76%. Although this percentage needs to be consistent w.r.t the atomic contents of the element used during synthesis. In order to further investigate this, EDX mapping was also conducted to analyze whether the composite is homogenous or heterogenous

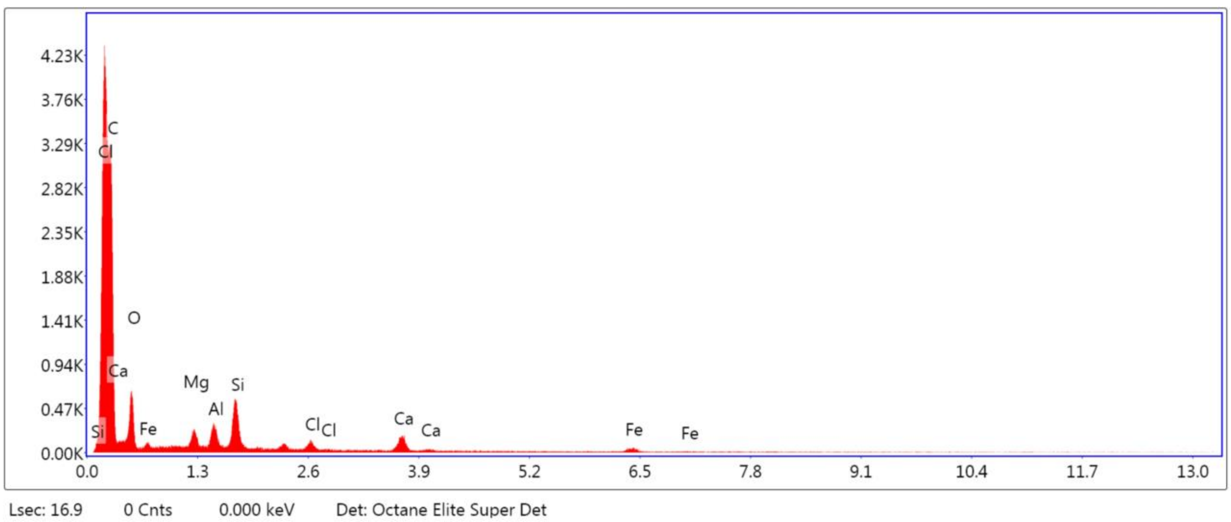

Figure 4.1: EDS analysis of Activated Carbon

Table 4.1: Weight and atomic percentages of elements present in Activated Carbon

Element	Weight %	Atomic %	Net Int.	Error %	K-ratio	Z	R	A	F
C K	70.29	78.60	2708.97	6.82	0.3393	1.0217	0.9882	0.4724	1.0000
O K	20.98	17.61	489.97	10.99	0.0257	0.9764	1.0071	0.1256	1.0000
MgK	1.43	0.79	208.24	8.04	0.0076	0.9005	1.0362	0.5876	1.0050
AlK	1.50	0.74	257.27	6.33	0.0095	0.8669	1.0423	0.7269	1.0071
SiK	2.60	1.24	497.98	4.27	0.0192	0.8857	1.0479	0.8284	1.0073
ClK	0.60	0.23	100.41	11.57	0.0050	0.8246	1.0629	0.9846	1.0238
CaK	1.63	0.55	197.30	7.06	0.0146	0.8352	1.0750	1.0287	1.0428
FeK	0.98	0.23	59.63	15.55	0.0087	0.7439	1.0894	1.0258	1.1659

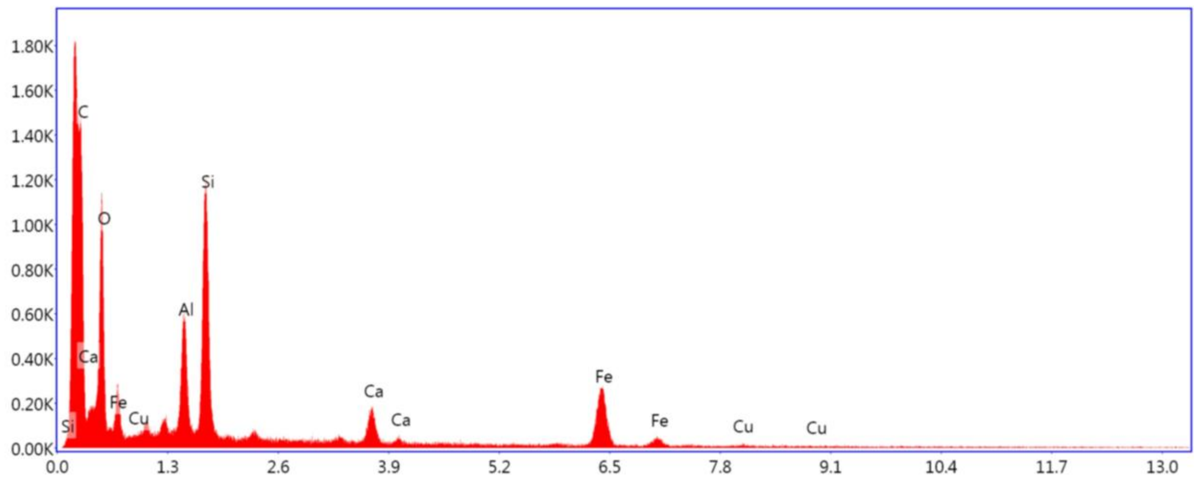

Figure 4.2: EDX analysis of Cu-1 (300⁰C)

Table 4.2: Weight and atomic percentages of elements present in Cu-1 (300⁰C)

Element	Weight %	Atomic %	Net Int.	Error %	K-ratio	Z	R	A
C K	57.47	69.61	1934.19	7.87	0.2196	1.0402	0.9768	0.3674
O K	26.23	23.85	812.24	10.46	0.0387	0.9949	0.9967	0.1482
AlK	2.89	1.56	519.63	5.84	0.0174	0.8845	1.0337	0.6748
SiK	5.26	2.73	1049.80	4.27	0.0368	0.9038	1.0397	0.7684
CaK	1.37	0.50	186.77	7.48	0.0125	0.8529	1.0686	1.0119
FeK	6.48	1.69	413.11	4.42	0.0546	0.7602	1.0847	1.0226
CuK	0.29	0.07	11.99	58.19	0.0025	0.7274	1.0846	1.0118

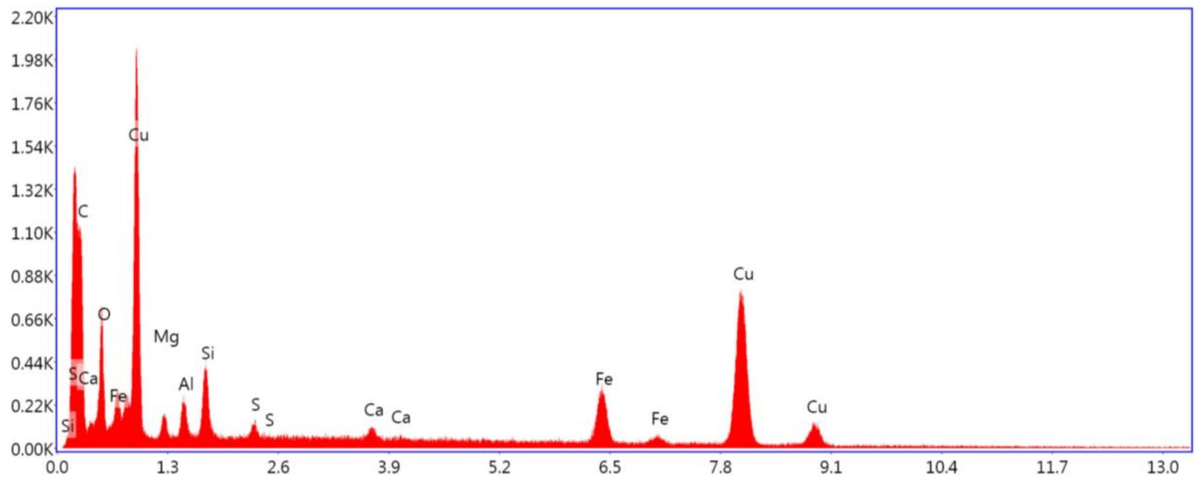

Figure 4.3: EDX analysis of Cu-1 (500^{o}C)

Table 4.3: Weight and atomic percentages of elements present in Cu-1 (500^{o}C)

Element	Weight %	Atomic %	Net Int.	Error %	K-ratio	Z	R	A
C K	40.06	66.83	1032.67	9.52	0.1150	1.1305	0.9202	0.2538
O K	12.24	15.32	525.28	10.39	0.0245	1.0854	0.9434	0.1845
MgK	1.65	1.36	144.77	11.84	0.0047	1.0071	0.9800	0.2824
AlK	1.52	1.13	181.07	11.28	0.0059	0.9706	0.9879	0.4004
SiK	2.19	1.56	333.18	8.56	0.0114	0.9928	0.9953	0.5237
S K	0.32	0.20	56.91	19.24	0.0023	0.9737	1.0090	0.7359
CaK	0.54	0.27	77.61	20.69	0.0051	0.9409	1.0324	0.9520
FeK	5.60	2.01	478.22	5.85	0.0619	0.8419	1.0569	1.0102
CuK	35.88	11.32	1496.24	2.88	0.3066	0.8076	1.0618	1.0059

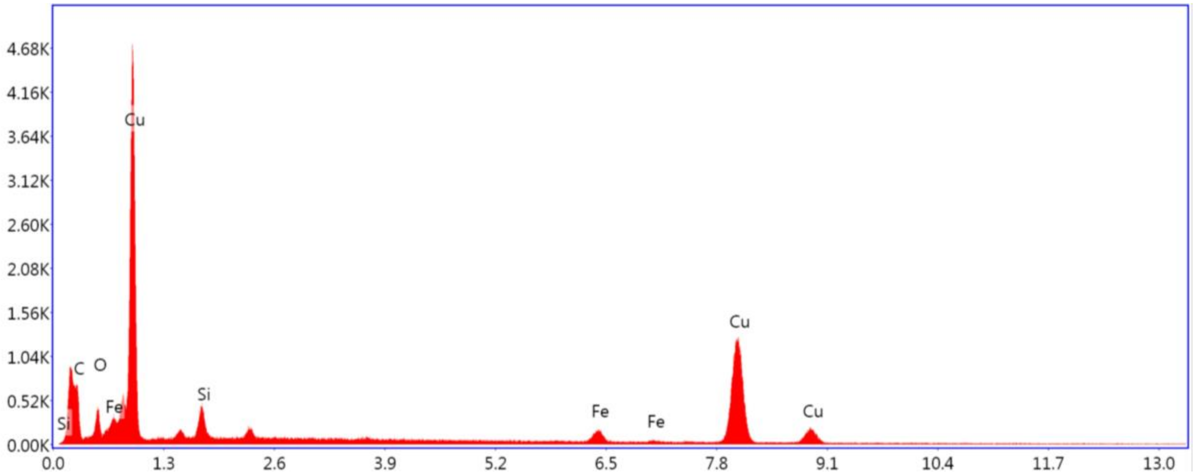

Figure 4.4: EDX analysis EDX analysis of Cu-1 (700ºC)

Table 4.4: Weight and atomic percentages of elements present in Cu-1 (700ºC)

Element	Weight %	Atomic %	Net Int.	Error %	K-ratio	Z	R	A
C K	36.69	69.51	1029.34	9.49	0.1011	1.1670	0.8994	0.2362
O K	6.17	8.78	322.79	10.99	0.0133	1.1215	0.9234	0.1921
SiK	2.51	2.03	407.11	8.71	0.0123	1.0278	0.9775	0.4759
FeK	2.24	0.91	250.54	10.91	0.0286	0.8742	1.0447	1.0062
CuK	52.39	18.76	2560.71	2.61	0.4635	0.8395	1.0515	1.0079

Figure 4.5 to Figure 4.9 show EDX graphs of composites Cu-2, Cu-0.5, Cu-0.25, Cu-0.125 and Cu-0 respectively, all of which were synthesized at 500ºC. Table 4.5 to Table 4.9 show the weight and atomic percentages of elements of the composites Cu-2, Cu-0.5, Cu-0.25, Cu-0.125 and Cu-0 respectively. The presence of Carbon, iron and copper in these composites is confirmed by the graphs. Mass ratio of copper was varied and the EDS results indicate a direct relationship between the ratio of copper in the composite and the atomic percentage of copper in the EDS analysis.. The EDX data of Cu-0 shows presence of only carbon and iron.

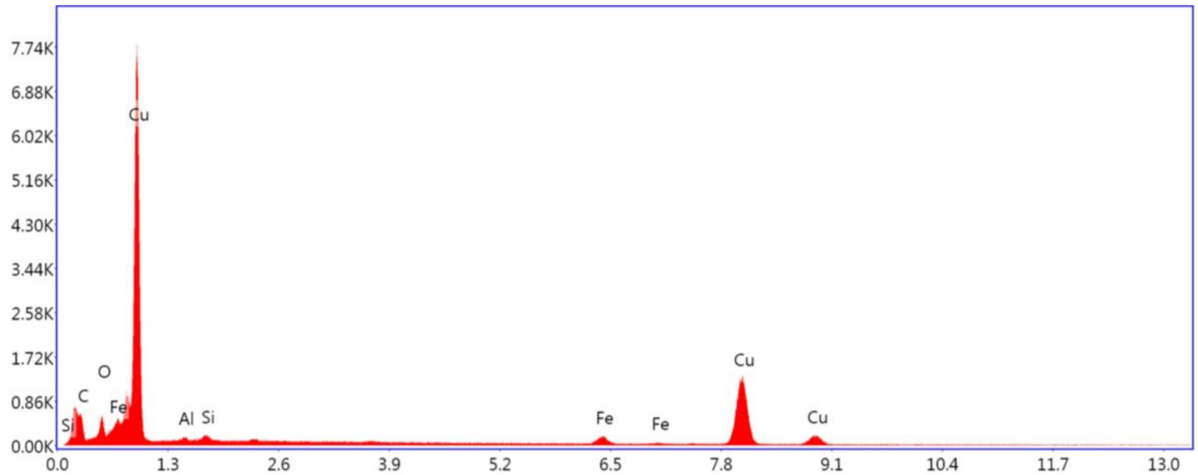

Figure 4.5: EDX analysis of Cu-2 (500ºC)

Table 4.5: Weight and atomic percentages of elements present in Cu-2 (500ºC)

Element	Weight %	Atomic %	Net Int.	Error %	K-ratio	Z	R	A
C K	31.05	62.69	896.88	9.78	0.0834	1.1816	0.8929	0.2272
O K	8.47	12.84	520.04	10.48	0.0202	1.1358	0.9170	0.2103
AlK	1.34	1.20	166.53	12.64	0.0045	1.0178	0.9639	0.3330
SiK	1.17	1.01	192.50	11.23	0.0055	1.0414	0.9718	0.4509
FeK	2.48	1.08	297.92	10.17	0.0321	0.8864	1.0406	1.0048
CuK	55.49	21.18	2915.89	2.59	0.4971	0.8515	1.0480	1.0068

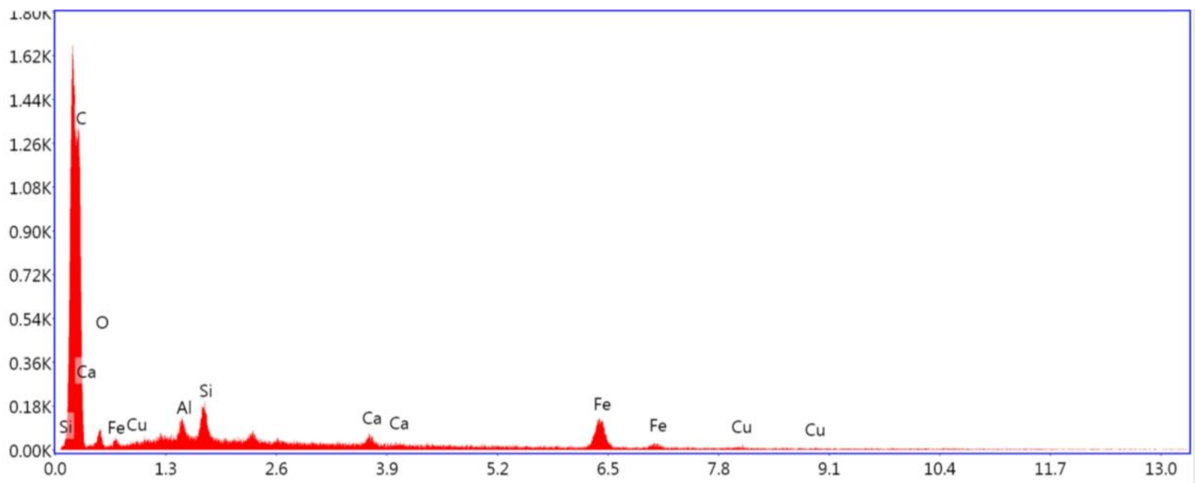

Figure 4.6: EDX analysis of Cu-0.5 (500^{o}C)

Table 4.6: Weight and atomic percentages of elements present in Cu-0.5 (500^{o}C)

Element	Weight %	Atomic %	Net Int.	Error %	K-ratio	Z	R	A
C K	84.33	93.01	1624.36	5.42	0.5310	1.0241	0.9837	0.6149
O K	4.73	3.91	36.80	17.88	0.0050	0.9791	1.0029	0.1089
AlK	0.52	0.25	34.06	23.01	0.0033	0.8700	1.0388	0.7205
SiK	1.25	0.59	93.36	11.13	0.0094	0.8890	1.0446	0.8348
CaK	0.79	0.26	38.35	22.76	0.0074	0.8388	1.0724	1.0353
FeK	7.84	1.86	171.69	7.21	0.0651	0.7476	1.0875	1.0277
CuK	0.54	0.11	7.48	59.93	0.0045	0.7154	1.0869	1.0128

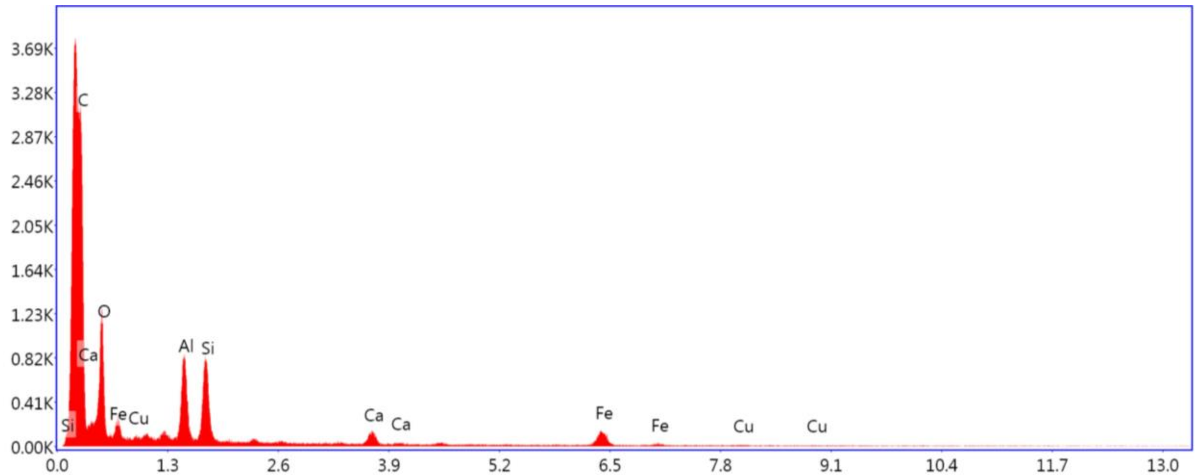

Figure 4.7: EDX analysis of Cu-0.25 (500^{o}C)

Table 4.7: Weight and atomic percentages of elements present in Cu-0.25 (500^{o}C)

Element	Weight %	Atomic %	Net Int.	Error %	K-ratio	Z	R	A
C K	67.88	76.49	4443.83	6.39	0.3405	1.0238	0.9871	0.4899
O K	23.89	20.21	976.04	10.52	0.0318	0.9785	1.0061	0.1360
AlK	2.58	1.30	710.81	5.08	0.0165	0.8689	1.0414	0.7311
SiK	2.40	1.16	720.28	4.23	0.0176	0.8877	1.0471	0.8178
CaK	0.74	0.25	142.95	10.05	0.0067	0.8372	1.0743	1.0280
FeK	2.29	0.55	216.83	6.39	0.0201	0.7458	1.0889	1.0259
CuK	0.22	0.05	14.07	58.40	0.0021	0.7134	1.0880	1.0175

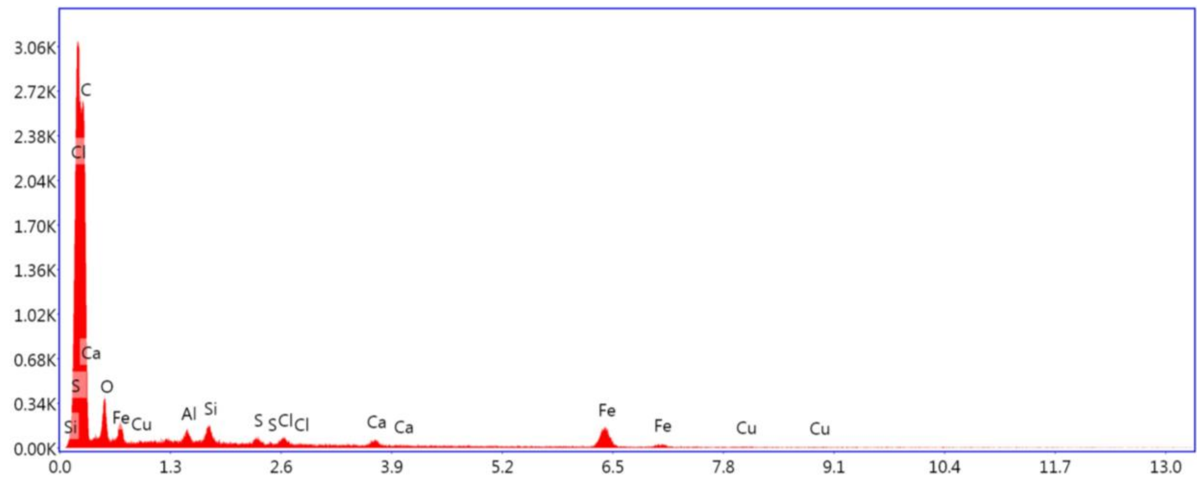

Figure 4.8: EDX analysis of Cu-0.125 (500^{o}C)

Table 4.8: Weight and atomic percentages of elements present in Cu-0.125 (500^{o}C)

Element	Weight %	Atomic %	Net Int.	Error %	K-ratio	Z	R	A
C K	61.19	71.04	3336.46	7.03	0.2740	1.0298	0.9840	0.4349
O K	27.76	24.20	1153.43	10.24	0.0402	0.9844	1.0032	0.1470
NaK	0.79	0.48	88.31	13.00	0.0027	0.8932	1.0263	0.3772
MgK	0.74	0.43	150.23	9.84	0.0037	0.9083	1.0329	0.5455
AlK	2.21	1.14	546.24	5.68	0.0136	0.8744	1.0391	0.6957
SiK	3.16	1.57	867.04	4.16	0.0225	0.8934	1.0449	0.7937
CaK	1.02	0.36	185.74	9.23	0.0093	0.8427	1.0726	1.0220
FeK	3.12	0.78	272.63	5.80	0.0269	0.7508	1.0877	1.0245

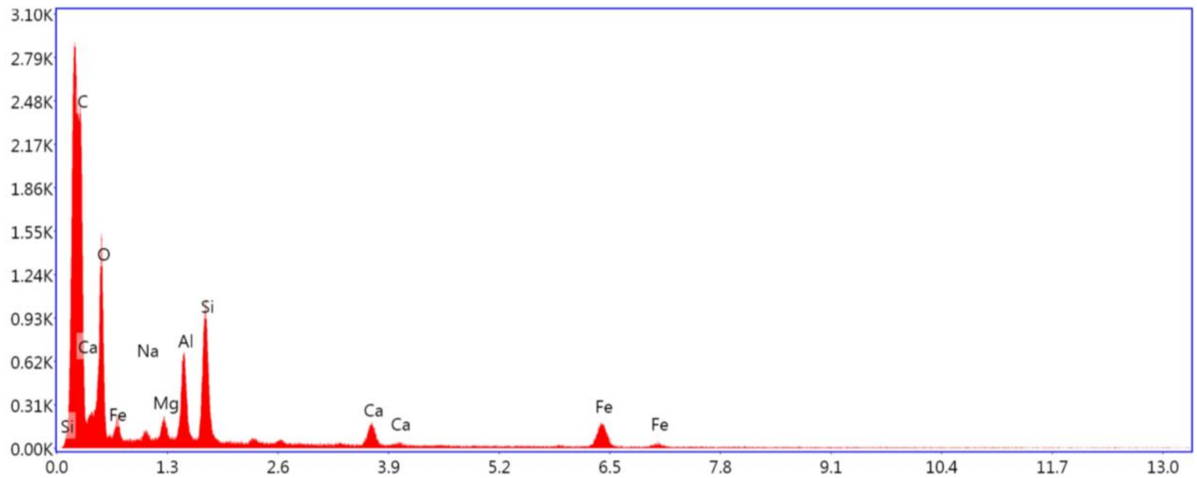

Figure 4.9: EDX analysis of Cu-0 (500^{o}C)

Table 4.9: Weight and atomic percentages of elements present in Cu-0 (500^{o}C)

Element	Weight %	Atomic %	Net Int.	Error %	K-ratio	Z	R	A
C K	40.06	66.83	1032.67	9.52	0.1150	1.1305	0.9202	0.2538
O K	12.24	15.32	525.28	10.39	0.0245	1.0854	0.9434	0.1845
MgK	1.65	1.36	144.77	11.84	0.0047	1.0071	0.9800	0.2824
AlK	1.52	1.13	181.07	11.28	0.0059	0.9706	0.9879	0.4004
SiK	2.19	1.56	333.18	8.56	0.0114	0.9928	0.9953	0.5237
S K	0.32	0.20	56.91	19.24	0.0023	0.9737	1.0090	0.7359
CaK	0.54	0.27	77.61	20.69	0.0051	0.9409	1.0324	0.9520
FeK	5.60	2.01	478.22	5.85	0.0619	0.8419	1.0569	1.0102
CuK	35.88	11.32	1496.24	2.88	0.3066	0.8076	1.0618	1.0059

In order to confirm the distribution (homogenous or heterogenous) of iron and copper on activated carbon, EDX mapping was performed. Figure 4.10 to Figure 4.17 show EDS mapping of the eight synthesized composites. These images confirm that the synthesized composites are heterogenous as the iron and copper are not homogenously dispersed, which is also supported by the EDS analysis explained earlier.

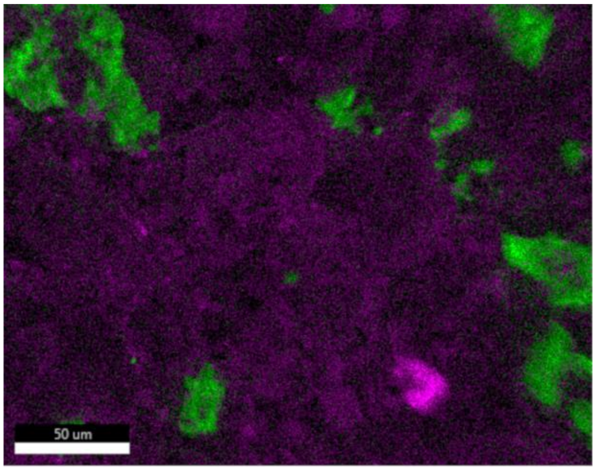

Figure 4.10: EDX mapping of Cu-1, synthesized at 300^oC

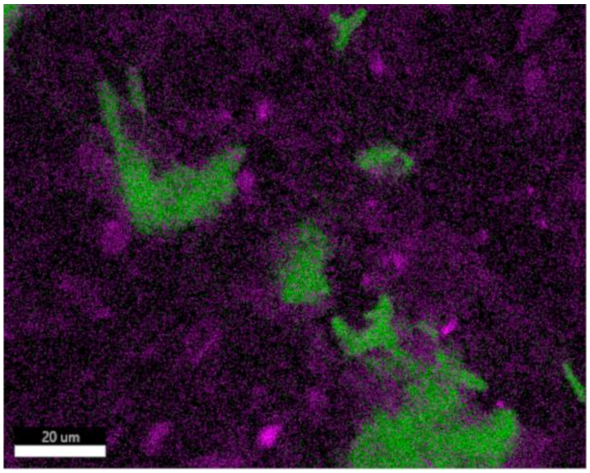

Figure 4.11: EDX mapping of Cu-1, synthesized at 500^oC

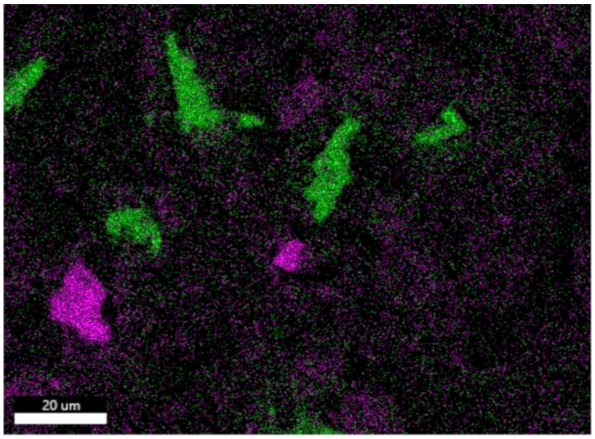

Figure 4.12: EDX mapping of Cu-1, synthesized at 700^oC

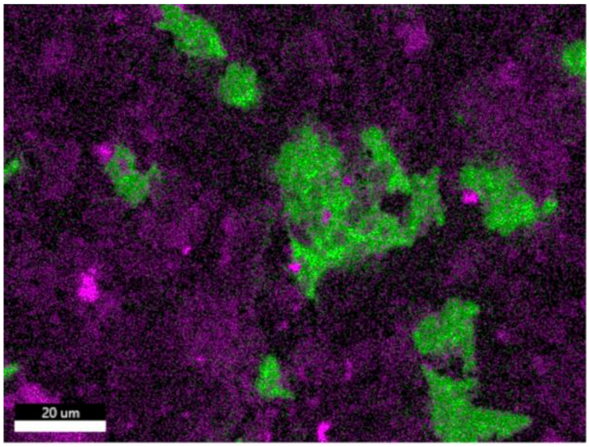

Figure 4.13: EDX mapping of Cu-2, synthesized at 500^oC

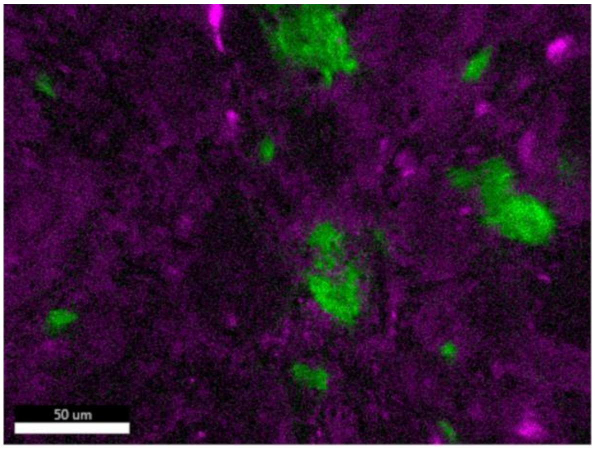

Figure 4.14: EDX mapping of Cu-0.5, synthesized at 500^{o}C

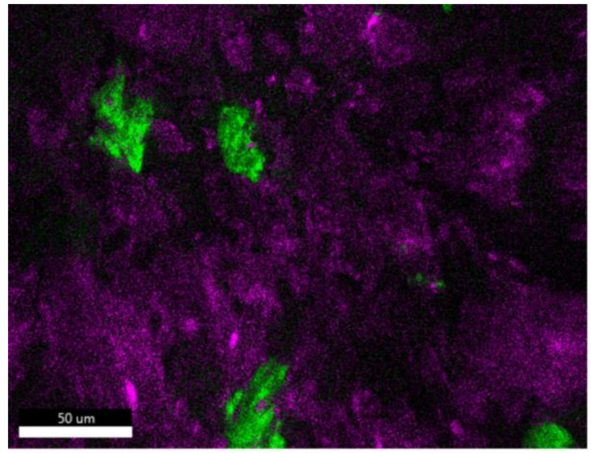

Figure 4.15: EDX mapping of Cu-0.25, synthesized at 500^{o}C

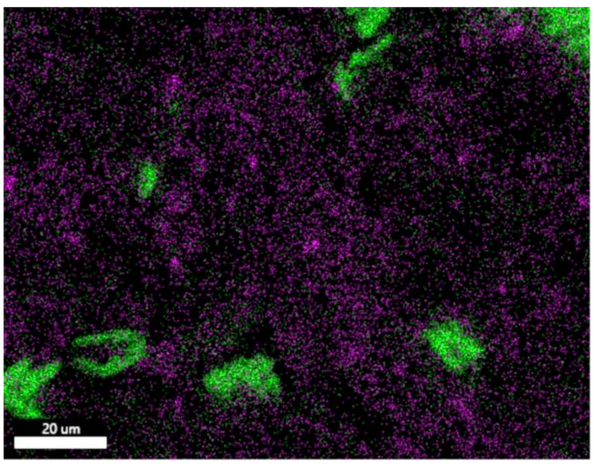

Figure 4.16: EDX mapping of Cu-0.125, synthesized at 500^{o}C

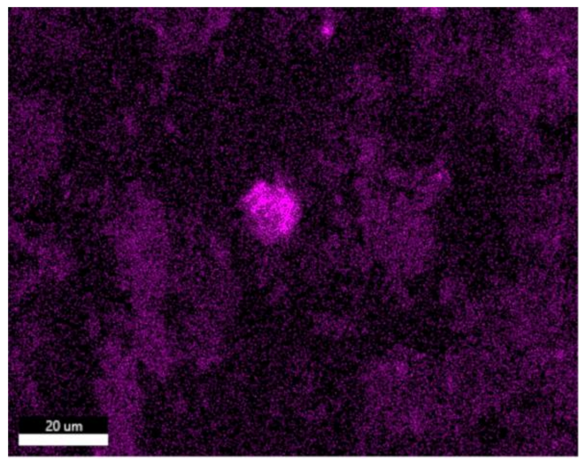

Figure 4.17: EDX mapping of Cu-0, synthesized at 500^{o}C

4.1.2 Scanning Electron Microscopy (SEM)

SEM analysis is employed for identification of structural arrangements and morphology of the Lab grade activated carbon, used for synthesis of composite, and for the synthesized composites. The acceleration voltage was set at 20kV and the analysis was performed at SCME, NUST. Figure 4.18

illustrates SEM image of Activated Carbon. Figure 4.19 to Figure 4.26 illustrates the SEM images of composites Cu-2, Cu-0.5, Cu-0.25, Cu-0.125 and Cu-0 respectively.

As shown in figure 4.19, Activated Carbon exhibited heterogenous structure with numerous pores on the surface which provides effective attachment sites for Fe and Cu. Figure 4.20 is SEM image of Cu-1 synthesized at 300ºC which also exhibits heterogenous structure with irregular pores. Metal particles can be seen adhered to the surface of activated carbon. Figure 4.21 shows SEM image of Cu-1 synthesized at 500ºC which shows increase in porosity as large metal particles are dispersed and adhered on the surface. Figure 4.22 shows SEM image of Cu-1 synthesized at 700 and it can be seen that there is decrease in porosity of the composite as compared to one synthesized at 500 degrees Celsius. After sintering, composite presented enhanced porous structure which increased the specific surface area to provide abundant active sites for oxidation reduction reaction. Iron and copper can be seen adhered to the surface. When the synthesis temperature increased from 300 to 500 degrees Celsius, composite showed enhancement in the surface structure. Though as the synthesis temperature rises from 500 to 700 degrees Celsius, pores decreased. Hence 500ºC was selected as the optimum temperature for sintering

Figure 4.23 and Figure 4.24 are SEM images of Cu-2 and Cu-0.5 respectively. They both exhibited heterogenous structure with porous texture. It can be clearly seen that Cu-0.5 has less metallic loading on its surface. Figure 4.25 is SEM image of Cu-0.25, which exhibited most well-developed structure. Metals particles are scattered across the surface. The composite shows numerous pores on which organic pollutants are adsorbed and oxygen is reduced. Figure 4.26 shows SEM image of Cu-0.125 which exhibited an irregular porous structure. The dispersion of metals on the surface is uneven. Figure 4.27 is the SEM image of Cu-0. Fe metal is adhered to the surface however, its distribution is uneven as clusters of metals can be seen. Among the synthesized composites, Cu-

0.25 exhibited the most porous structure. It can be seen that iron and copper particles are well dispersed on the surface of activated carbon. This good dispersion of iron and copper will enlarge its surface area providing better catalysis for hydrogen peroxide to produce hydroxyl radicals to augment the Fenton-like effect

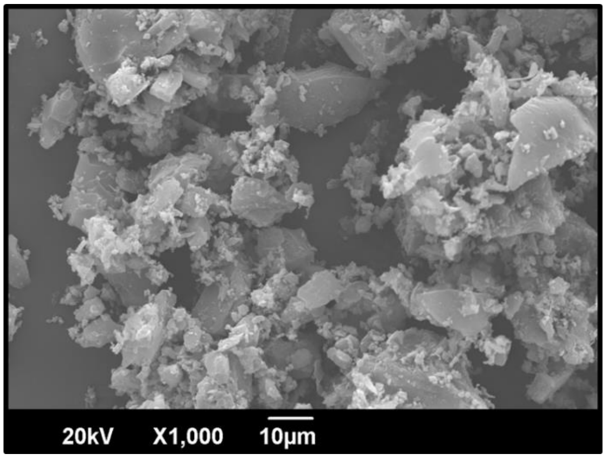

Figure 4.18: SEM of Activated Carbon

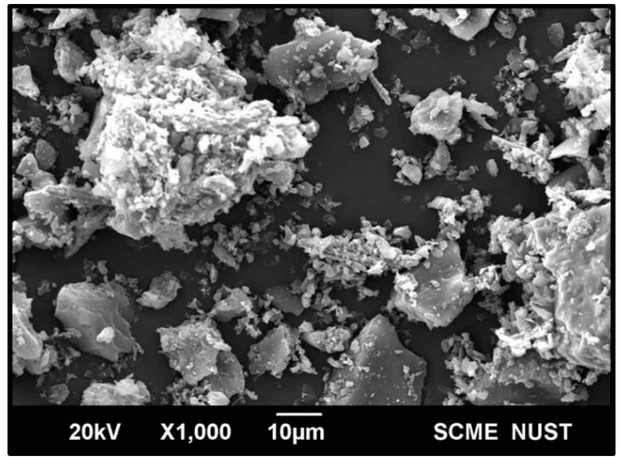

Figure 4.19: SEM of Cu-1, synthesized at 300⁰C

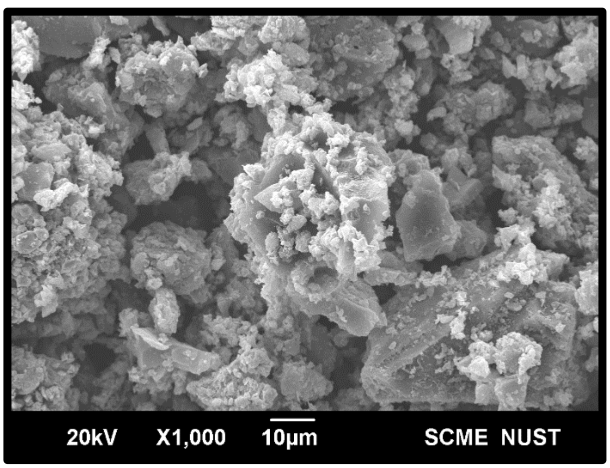

Figure 4.20: SEM of Cu-1, synthesized at 500⁰C

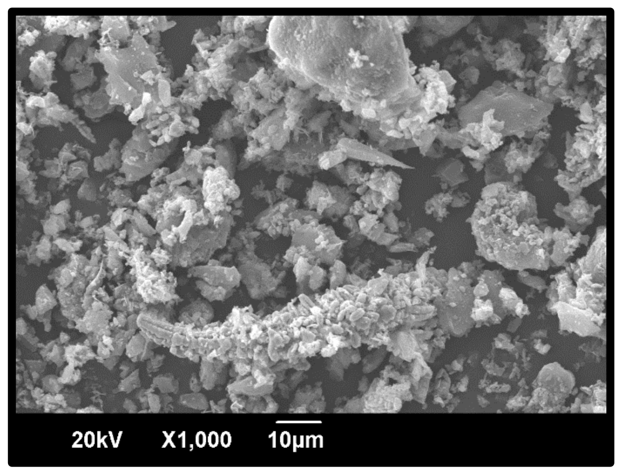

Figure 4.21: SEM of Cu-1, synthesized at 700⁰C

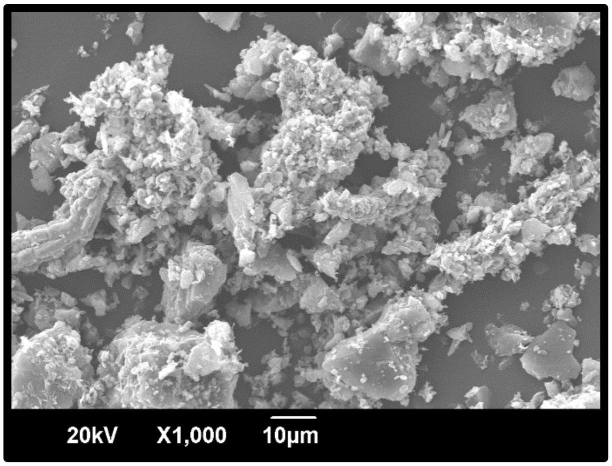

Figure 4.22: SEM of Cu-2, synthesized at 500⁰C

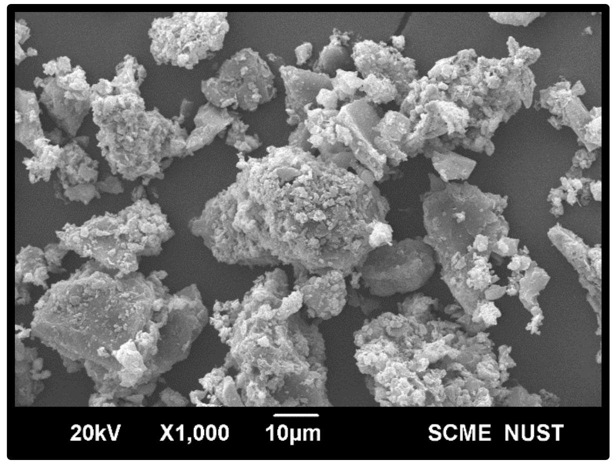

Figure 4.23: SEM of Cu-0.5, synthesized at 500⁰C

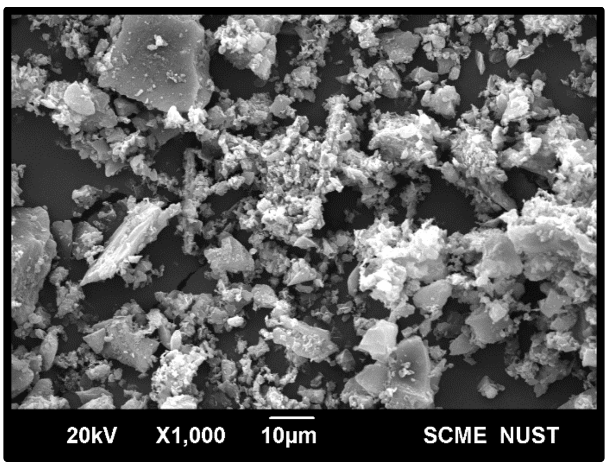

Figure 4.24: SEM of Cu-0.25, synthesized at 500⁰C

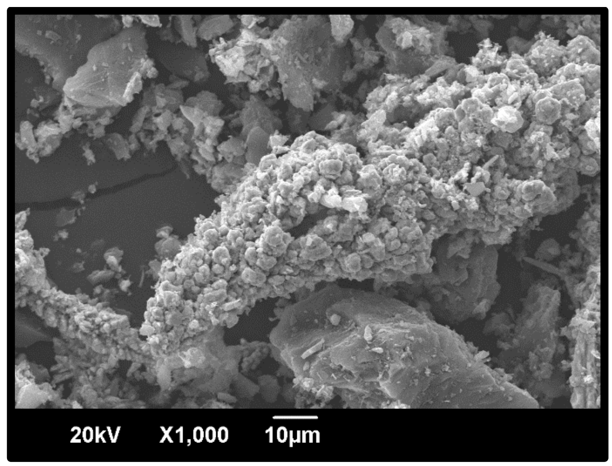

Figure 4.25: SEM of Cu-0.125, synthesized at 500⁰C

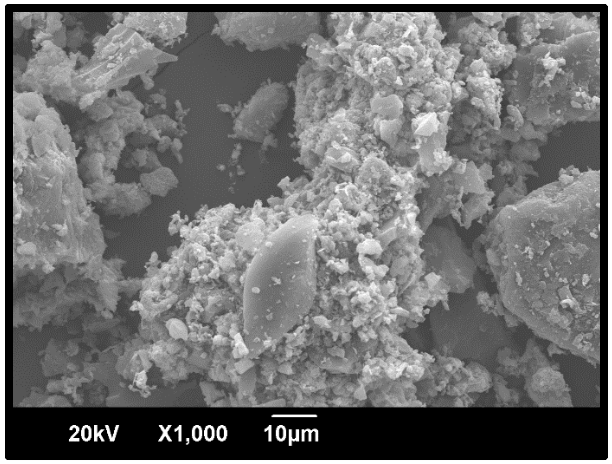

Figure 4.26: SEM of Cu-0, synthesized at 500ºC

4.1.3 X-ray Diffraction (XRD) analysis

XRD analysis was conducted to probe crystal structure of composites over a 2θ range of 0º - 120º. These analyses were performed at PIEAS. Figure 4.27 shows the XRD patterns of activated carbon and Cu-1 synthesized at 300, 500 and 700 degrees Celsius. the XRD graphs confirm the presence of carbon, iron and copper, as identified in EDX analysis. Iron is identified in its elemental form whereas copper is identified in its elemental form as well as its oxide form (cupric oxide, CuO). The XRD pattern of activated carbon shows amorphous peak of carbon at 26.15º which correspond to 002 crystal plane and matches with the JCPDS 99-0057. The peaks identified at 43.3º and 89.6º show presence of iron which corresponds to 111 and 131 crystal planes respectively and match with JCPDS 87-0721. The peak identified at 50.58º shows the presence of copper in its elemental form which corresponds to 200 crystal plane and match with the JCPDS 04-0836. The peak identified at 74.2º shows presence of copper oxide assigned to 220 crystal plane which matches with the JCPDS 74-1230. The composites exhibit well developed crystalline structure. While synthesis temperature rises from 300 to 500 degrees Celsius, the crystallinity of composite increases, where as it decreases slightly when synthesis temperature increases from 500ºC to 700ºC. Hence, 500ºC was selected as the optimum temperature.

Figure 4.28 shows XRD patterns of activated carbon and the composites synthesized at different ratios of copper. Among these, Cu-0.25 shows most well-developed peaks. Hence this composite was selected for treatment and optimization.

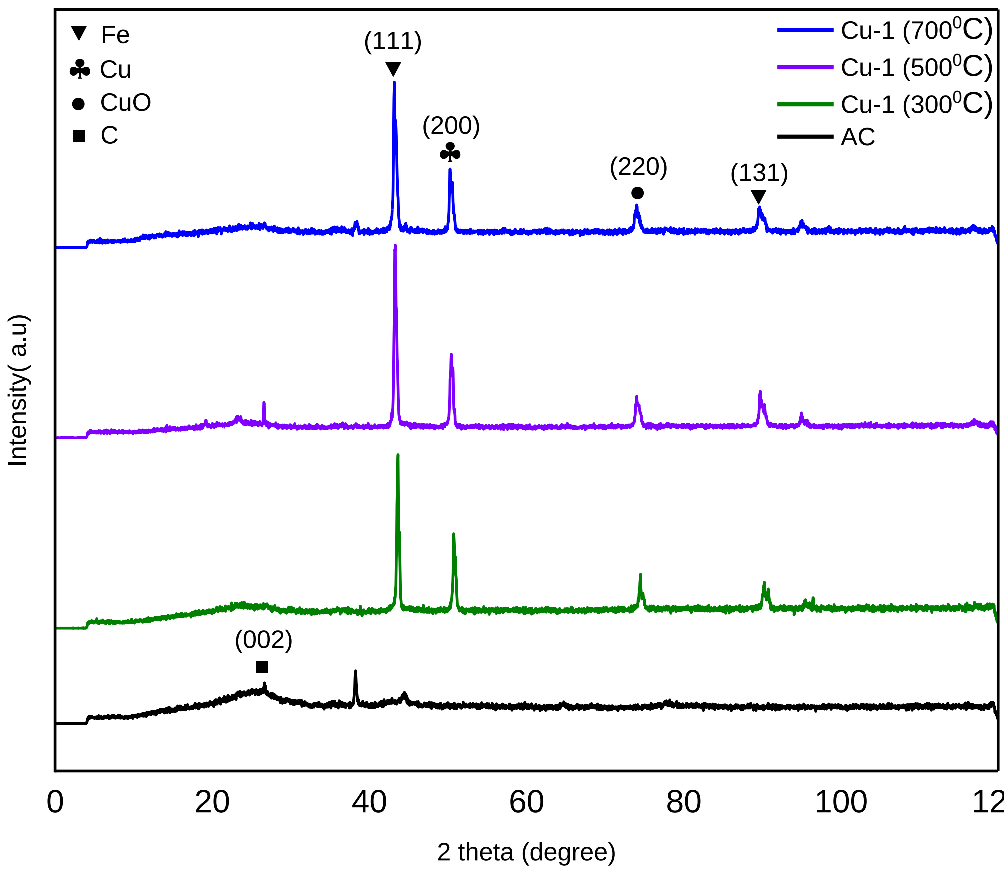

Figure 4.27: XRD pattern of Activated carbon and Cu-1 synthesized at 300ºC, 500ºC and 700ºC

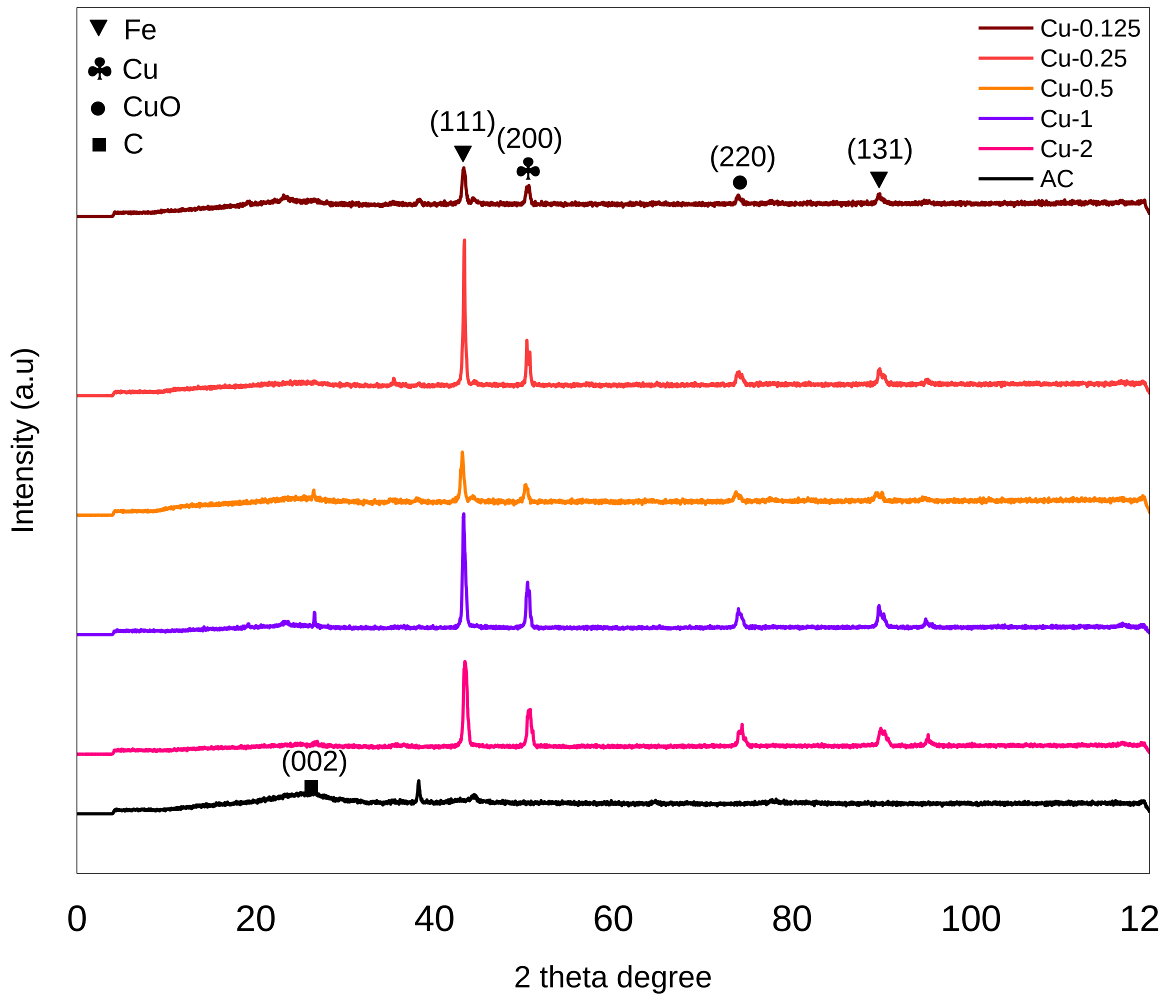

Figure 4.28: XRD pattern of Activated carbon and Cu-2, Cu-1, Cu-0.5, Cu-0.25, Cu-0.125 synthesized at 500°C

4.1.4 BET Analysis

Textural Properties of composites were determined by employing adsorption-desorption isotherms of nitrogen at 77K with the use of surface area and pore size analyzer. All the samples were degassed for 3 hours at 120°C. These analyses were performed at department of chemistry and chemical engineering at LUMS, Lahore. Figure 4.29 shows the N_2 adsorption/desorption isotherm of activated carbon. It depicts type 4 isotherm, according to IUPAC (International

Union of Pure and Applied Chemistry) classification, according to which large no. of mesopores are present on the surface of activated carbon. The pore size distribution was determined using Density Functional theory DFT method as presented in the Figure 4.30. The pore size of activated carbon is mostly distributed ranging from 3.5 to 18 nm and average pore width is 1.847 nm. The pore volume of activated carbon is 0.059 cm^3/g and the surface area is 90.98 m^2/g. The N_2 adsorption/desorption isotherm of Cu-0.25 also depicts type 4 isotherm, as shown in Figure 4.31 which suggests that large no. of mesopores are present on the surface of the composite. Figure 4.32 illustrates the pore size distribution of Cu-0.25 ranging of 2 to 18 nm and the average pore width is 1.932 nm. Pore volume of the composite is 0.099 cm^3/g and the surface area is 172.94 m^2/g. Surface area of composite is 90% more than the activated carbon because of the higher pore volume and pore size which is 60% more than that of activated carbon. Large surface area and porosity of the composite suggests that the composite would give high removal efficiency of the organic contaminants.

Table 4.10: Surface area, pore volume and pore size of Activated Carbon and Cu-0.25

	Activated Carbon	**Cu-0.25**
Surface Area (m^2/g)	90.98	172.94
Pore Volume (cm^3/g)	0.059	0.099
Pore size (nm)	1.847	1.932

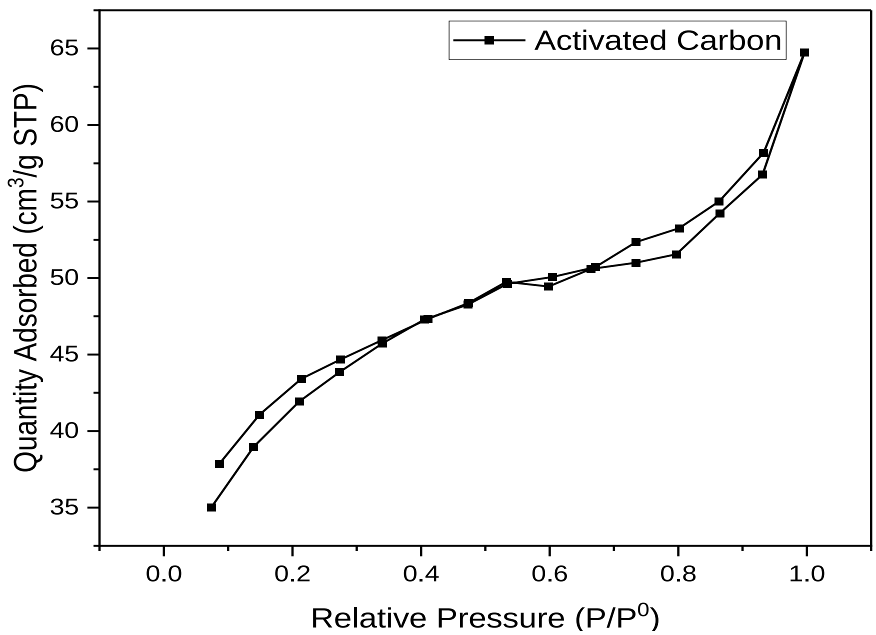

Figure 4.29: N_2 adsorption/desorption isotherm of Activated Carbon

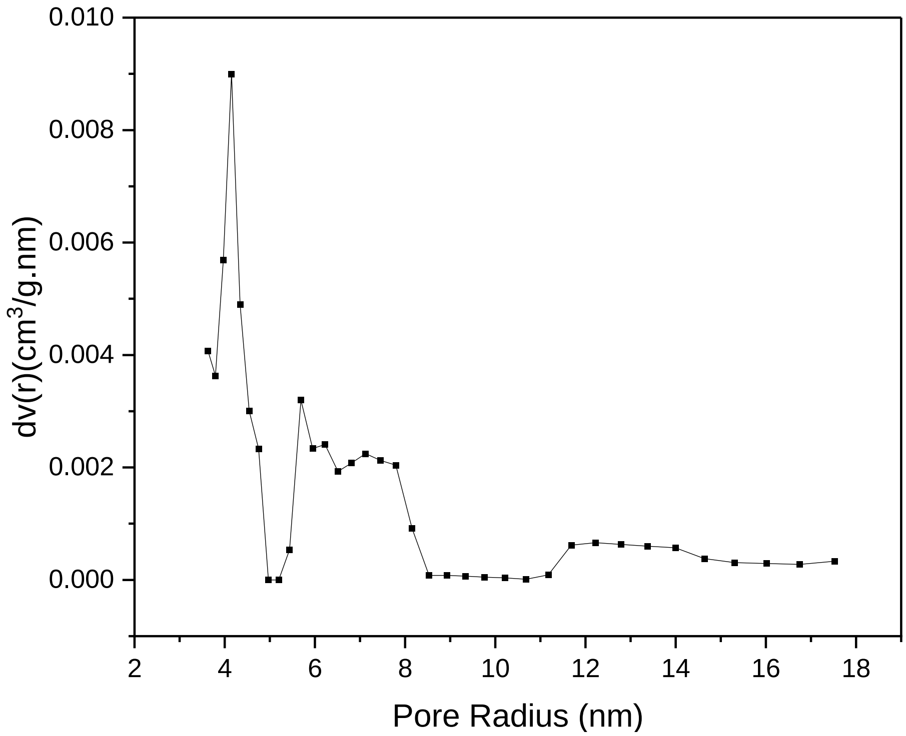

Figure 4.30: Pore Size Distribution of Activated Carbon

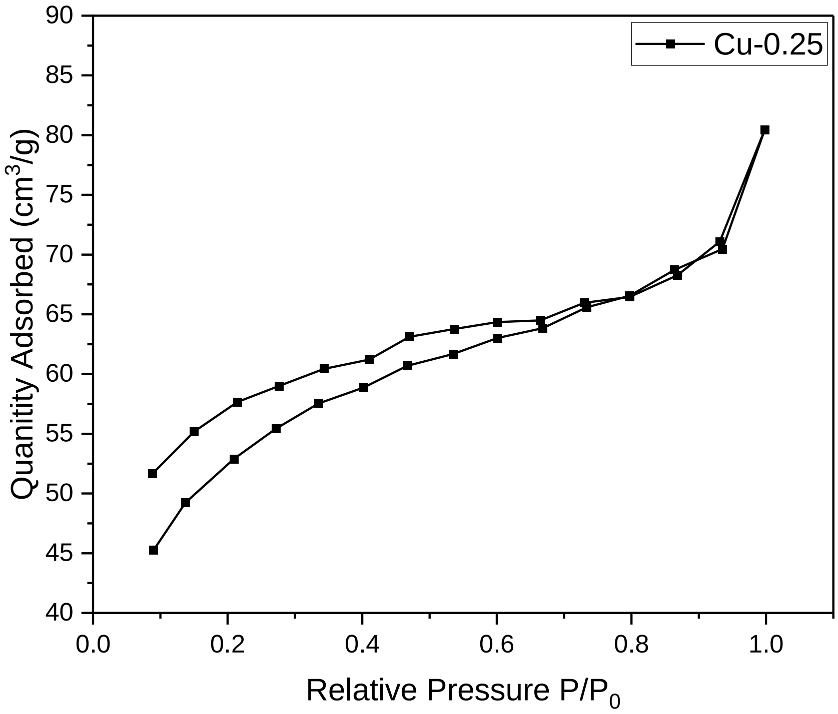

Figure 4.31: N_2 adsorption/desorption isotherm of Cu-0.25

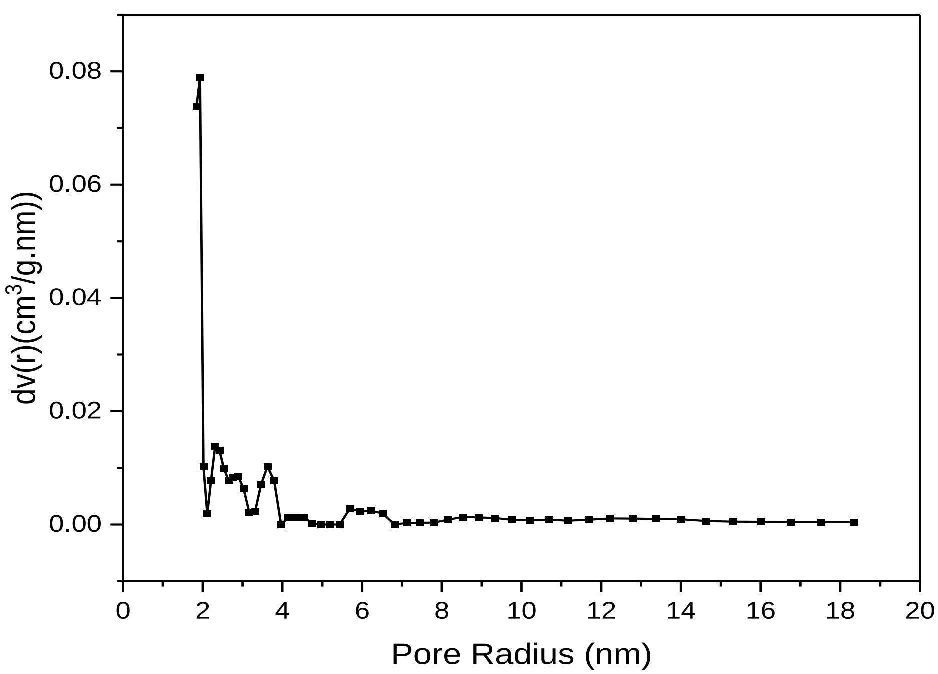

Figure 4.32: Pore Size Distribution of Cu-0.25

4.2 Degradation Experiments

4.2.1 Selection of optimum sintering temperature

Batch degradation experiments for methylene blue were carried out for selection of optimum sintering temperature for composite synthesis. Initially Cu-1 synthesized at 300, 500 and 700 degrees Celsius were tested for degradation of Methylene Blue. Initial conditions were kept constant as shown as shown in Table 4.11. After degradation of MB by these three composites, the results were plotted as shown in the bar graph in Figure 4.33. The synthesis conducted at 500 degree Celsius gave highest removal efficiency. It achieved a removal of 85.7% after 2 hours. Hence all other composites were synthesized at 500ºC

Table 4.11: Initial experimental conditions for degradation experiments

Composite Dosage	1g/L
Methylene Blue Concentration	50 mg/L
pH	4
Reaction Time	2 hours
Reaction volume	50ml
Temperature	Room Temperature

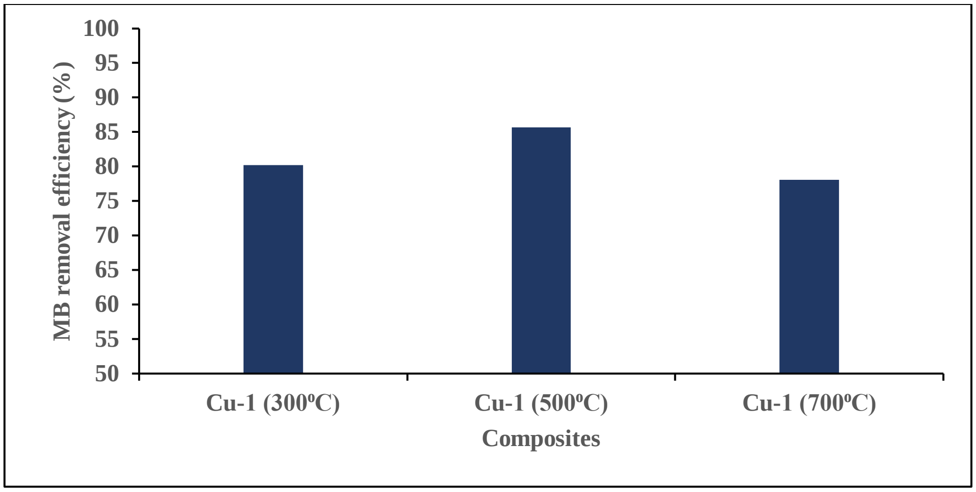

Figure 4.33: Removal efficiency of Cu-1 synthesized at 300ºC, 500ºC and 700ºC

4.2.2 Selection of optimum Copper concentration in the composite

Five more composites were synthesized while varying mass ratio of copper, at 500ºC. These composites were also evaluated for the degradation efficiency under the same initial conditions as shown in Table 411. Among these composites, Cu-0.25 degraded the pollutant most effectively. It gave removal of 93% within the first 60 mins and 97.5% removal after 120 mins. The least efficient composite was the one which had no copper i.e., Cu-1. It gave a removal of 81% after 120 mins.

Figure 4.34 shows removal efficiency of all the composites. All the composites gave removal of more than 55% in the first 30 minutes. Cu-0.25 was selected for further optimization.

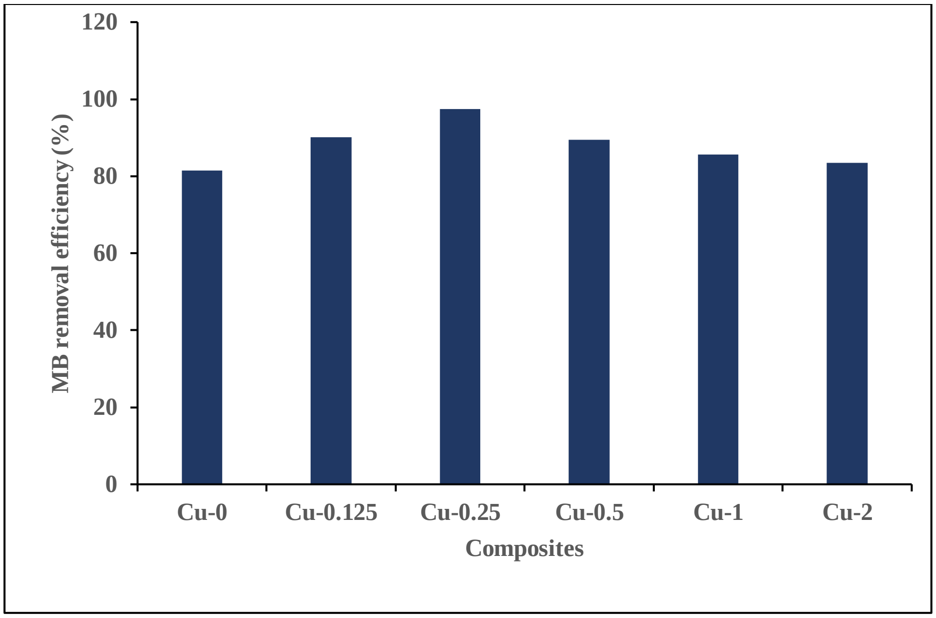

Figure 4.34: Removal efficiency of AC-Fe-Cu composites.

4.2.3 H_2O_2 Generation by AC-Fe-Cu Composites

H_2O_2 generation was measured using a spectrophotometer. Figure 4.35 shows in-situ H_2O_2 generation by different composites. The highest concentration of H_2O_2 was generated by Cu-0.25, which is 12.2mg/L after 2 hours. Hence it is the most effective composite among the composites synthesized in this study.

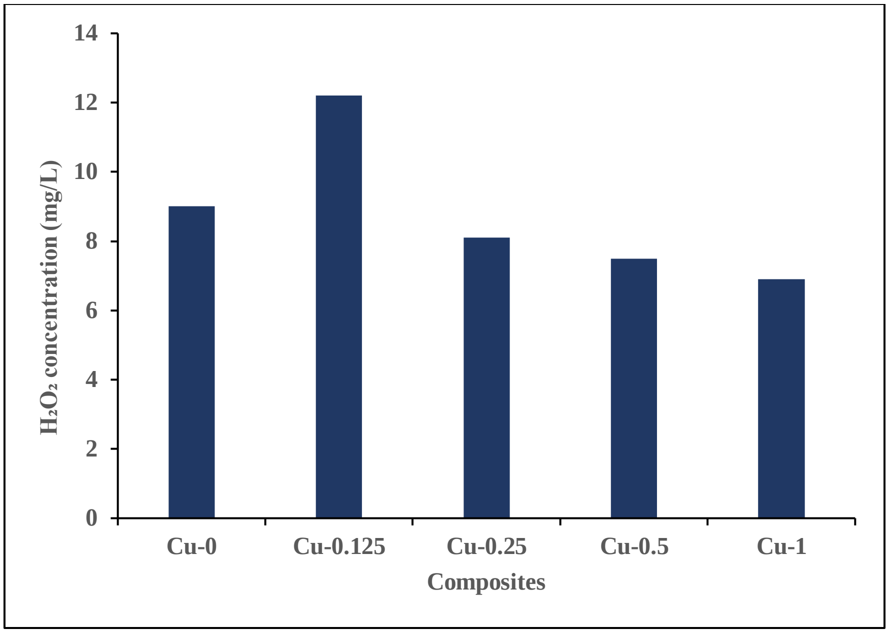

Figure 4.35: In-situ H_2O_2 generation

4.2.4 Optimization of selected composite

A number of degradation experiments were conducted to study the effect of composite dosage, pH and pollutant concentration on degradation of methylene blue. When determining the effect of each, all other parameters except the one being optimized were kept constant.

4.2.4.1 Composite dosage

Composite dose is a critical constraint influencing the degradation capacity of a composite under given pollutant concentration and operating conditions. When determining the effect of Composite dosage, all other parameters including the pH, Pollutant concentration, reaction time and reaction volume were kept constant at 4, 50mg/L, 2 hours and 50 mL respectively. Composite dosage was varied from 1g/L to 3g/L. Cu-0.25 gave a removal of 98.2% after 30 mins of treatment at a composite dosage of 3.0g/L. After 120 mins the removal achieved was 99.6%. Figure 4.36 illustrates capacity of synthesized composite to degrade the pollutant (gram of pollutant removed per gram of composite used). It can be seen from the graph that as the composite dose increases, removal capacity decreased. This was attributed to the fact that for a particular initial concentration of composite, available sites for reaction and surface area was larger and the intensity of pollutant loaded onto the unit surface area was lower. Therefore 1g/L was chosen as optimum dose and used for further experiments.

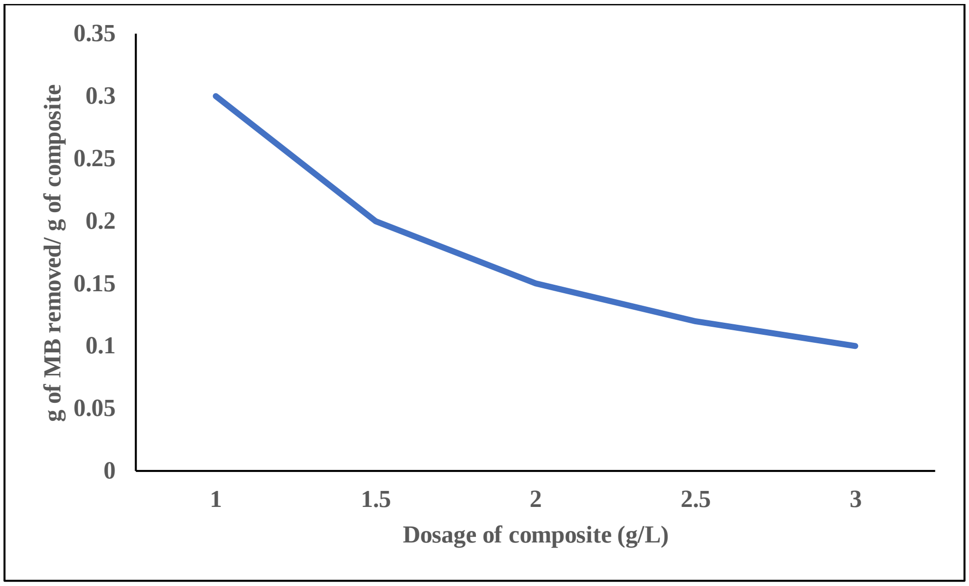

Figure 4.36: Effect of composite dosage

4.2.4.2 pH

When determining the effect of pH, all other parameters including the composite dosage, pollutant concentration, reaction time and reaction volume were kept constant. pH was varied from 1 to 7. Cu-0.25 gave a removal of 98.3% after 30 mins of treatment at pH 1. After 120 mins the removal achieved was 99.6%. Whereas at pH 7, 95.9% removal of Methylene Blue was achieved after 30 mins. pH of solution did not affect the capacity of the composite to degrade Methylene blue which can be depicted from the graph in Figure 4.37. The capacity of the composite decreased slightly after pH 4. The best removal efficiency was achieved at pH 1, but to make the process more economical pH 4 was selected to conduct further experiments. Removal of Methylene Blue is more efficient at lower pH because of availability of more H+ ions for formation of H_2O_2. Moreover, reactivity of iron is more at lower pH. However, the graph in Figure 4.37 shows that the composite can give good removal efficiency over a broad range of pH, due to presence of copper

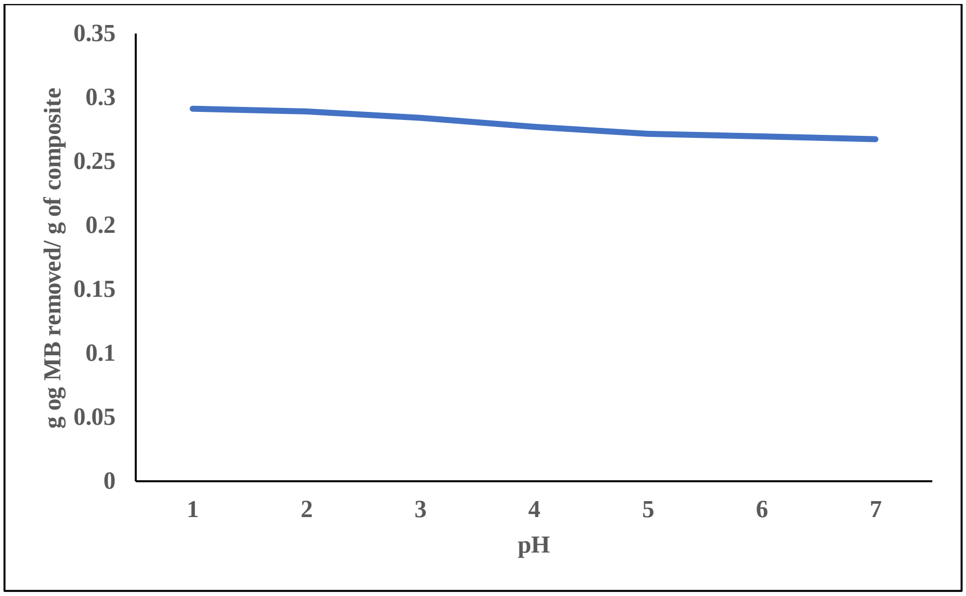

Figure 4.37: Effect of pH

4.2.4.3 Effect of Pollutant Concentration

When determining the impact of pollutant concentration, all other parameters including the pH, composite dosage, reaction time and reaction volume were kept constant. Pollutant concentration was varied from 10 mg/L of MB to 50 mg/L of MB. Cu-0.25 had the least efficiency while degrading a MB concentration of 10mg/l. It gave a removal of 86.4% after 30 mins and 92.3% removal after 120 mins. The composite degraded MB at a concentration of 40mg/L most efficiently with 92.4% removal after 30 mins and 97.2% removal at 120 mins after treatment. Although the capacity of the composite to degrade MB increases as the pollutant concentration augmented from 10mg/L to 50 mg/L as shown in the graph in Figure 4.38. The increase in degradation capacity results from higher pollutant concentration, because a higher driving force is applied by the pollutant which can overcome mass transfer resistance. This ultimately results in high MB being adsorbed on the surface and oxidized.

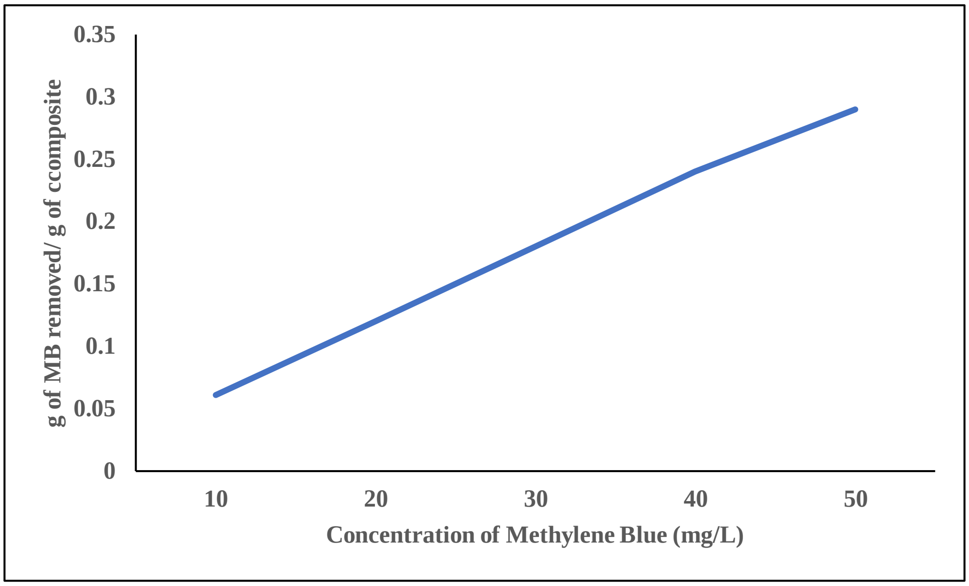

Figure 4.38:Effect of pollutant concentration

5 Conclusion and Recommendations

The AC-Fe-Cu composite is effective for treatment of emerging organic pollutants including dyes, antibiotics and persistent organic pollutants as this composite degrades organic pollutants by oxidation. The advantage of using this composite is that it is cost effective and ensure complete mineralization of pollutants. It is versatile as it performs well over a wide range of pH, including neutral pH. It gives a good removal efficiency even at low dose of 1g/L. Low concentrations of methylene blue give almost complete removal within 30 mins of treatment. High composite dosage is effective for treatment of methylene blue with concentrations above 50mg/L. The composite that gave the most efficient removal Cu-0.25, sintered at 500ºC. Cu-0.25 had a large surface area of 172.94 m2/g, which is 90% more as compared to that of Activated Carbon. It presented better results for degradation of Methylene Blue at optimal conditions of composite dosage 1g/L and pH 4. Moreover, among all the synthesized composites Cu-0.25 had the highest concentration of In-situ generated H_2O_2 i.e., 12.2mg/L in 120 mins.

For future studies, potential of various carbonaceous materials should be investigated to be used as matrix materials such as graphene and CNTs. Potential of various metals to be used as catalysts for synthesis of composites should also be investigated, such as Zn, Al and Mg. Regeneration studies should also be performed for evaluation of cost-effectiveness and to make the process more economical. Furthermore, techno-economic assessment should be conducted for large scale production and commercialization of the composite.

6 References

Alnatt und A . B. Lidiard: (1995). 29281.

Arslan, I., & Balcioglu, I. A. (2001). Advanced oxidation of raw and biotreated textile industry wastewater with O3, H2O2/UV-C and their sequential application. *Journal of Chemical Technology and Biotechnology*, *76*(1), 53–60. https://doi.org/10.1002/1097-4660(200101)76:1<53::AID-JCTB346>3.0.CO;2-T

Asghar, A., Raman, A. A. A., & Daud, W. M. A. W. (2015). Advanced oxidation processes for in-situ production of hydrogen peroxide/hydroxyl radical for textile wastewater treatment: A review. *Journal of Cleaner Production*, *87*(1), 826–838. https://doi.org/10.1016/j.jclepro.2014.09.010

Bhatia, D., Sharma, N. R., Singh, J., & Kanwar, R. S. (2017). Biological methods for textile dye removal from wastewater: A review. *Critical Reviews in Environmental Science and Technology*, *47*(19), 1836–1876. https://doi.org/10.1080/10643389.2017.1393263

Biswas, A. K., & Tortajada, C. (2018). Assessing Global Water Megatrends. *Water Resources Development and Management*, *March*, 1–26. https://doi.org/10.1007/978-981-10-6695-5_1

Book Reviews. (1957). *Public Administration*, *35*(4), 419–430. https://doi.org/10.1111/j.1467-9299.1957.tb01322.x

Chen, Y., Yang, Z., Liu, Y., & Liu, Y. (2020). Fenton-like degradation of sulfamerazine at nearly neutral pH using Fe-Cu-. *Chemical Engineering Journal*, *396*(April), 125329. https://doi.org/10.1016/j.cej.2020.125329

Cheng, M., Lai, C., Liu, Y., Zeng, G., Huang, D., Zhang, C., Qin, L., Hu, L., Zhou, C., & Xiong,

W. (2018). Metal-organic frameworks for highly efficient heterogeneous Fenton-like catalysis. *Coordination Chemistry Reviews*, *368*, 80–92. https://doi.org/10.1016/j.ccr.2018.04.012

Cho, M., Chung, H., Choi, W., & Yoon, J. (2005). Different inactivation behaviors of MS-2 phage and Escherichia coli in TiO2 photocatalytic disinfection. *Applied and Environmental Microbiology*, *71*(1), 270–275. https://doi.org/10.1128/AEM.71.1.270-275.2005

Dollimore, D., Spooner, P., & Turner, A. (1976). The bet method of analysis of gas adsorption data and its relevance to the calculation of surface areas. *Surface Technology*, *4*(2), 121–160. https://doi.org/10.1016/0376-4583(76)90024-8

Fu, T., Gong, X., Guo, J., Yang, Z., & Liu, Y. (2021). Zn-CNTs-Cu catalytic in-situ generation of H2O2 for efficient catalytic wet peroxide oxidation of high-concentration 4-chlorophenol. *Journal of Hazardous Materials*, *401*(April 2020), 123392. https://doi.org/10.1016/j.jhazmat.2020.123392

Ganzenko, O., Huguenot, D., van Hullebusch, E. D., Esposito, G., & Oturan, M. A. (2014). Electrochemical advanced oxidation and biological processes for wastewater treatment: A review of the combined approaches. *Environmental Science and Pollution Research*, *21*(14), 8493–8524. https://doi.org/10.1007/s11356-014-2770-6

Glaze, W. H. (1987). Drinking-water treatment with ozone. *Environmental Science and Technology*, *21*(3), 224–230. https://doi.org/10.1021/es00157a001

Gong, X. bo, Yang, Z., Peng, L., Zhou, A. lan, Liu, Y. lan, & Liu, Y. (2018). In-situ synthesis of hydrogen peroxide in a novel Zn-CNTs-O2 system. *Journal of Power Sources*, *378*(November 2017), 190–197. https://doi.org/10.1016/j.jpowsour.2017.12.040

Gu, T., Dong, H., Lu, T., Han, L., & Zhan, Y. (2019). Fluoride ion accelerating degradation of organic pollutants by Cu(II)-catalyzed Fenton-like reaction at wide pH range. *Journal of Hazardous Materials*, *377*(May), 365–370. https://doi.org/10.1016/j.jhazmat.2019.05.073

Holkar, C. R., Jadhav, A. J., Pinjari, D. V., Mahamuni, N. M., & Pandit, A. B. (2016). A critical review on textile wastewater treatments: Possible approaches. *Journal of Environmental Management*, *182*, 351–366. https://doi.org/10.1016/j.jenvman.2016.07.090

Huang, C. P., Dong, C., & Tang, Z. (1993). Advanced chemical oxidation: Its present role and potential future in hazardous waste treatment. *Waste Management*, *13*(5–7), 361–377. https://doi.org/10.1016/0956-053X(93)90070-D

Ikai, H., Nakamura, K., Shirato, M., Kanno, T., Iwasawa, A., Sasaki, K., Niwano, Y., & Kohno, M. (2010). Photolysis of hydrogen peroxide, an effective disinfection system via hydroxyl radical formation. *Antimicrobial Agents and Chemotherapy*, *54*(12), 5086–5091. https://doi.org/10.1128/AAC.00751-10

James, D. . (2003). Microscopy techniques for materials science. *Polymer Testing*, *22*(6), 721. https://doi.org/10.1016/s0142-9418(03)00014-x

Khandare, R. V., & Govindwar, S. P. (2015). Phytoremediation of textile dyes and effluents: Current scenario and future prospects. *Biotechnology Advances*, *33*(8), 1697–1714. https://doi.org/10.1016/j.biotechadv.2015.09.003

Liu, Y., Fan, Q., Liu, Y., & Wang, J. (2018). Fenton-like oxidation of 4-chlorophenol using H2O2 in situ generated by Zn-Fe-CNTs composite. *Journal of Environmental Management*, *214*, 252–260. https://doi.org/10.1016/j.jenvman.2018.03.024

Liu, Y., Fan, Q., & Wang, J. (2018). *Zn-Fe-CNTs catalytic in situ generation of H 2 O 2 for Fenton-like degradation of sulfamethoxazole*. *342*, 166–176.

Liu, Y., Liu, Y., Yang, Z., & Wang, J. (2017). Fenton degradation of 4-chlorophenol using H2O2: In situ generated by Zn-CNTs/O2 system. *RSC Advances*, *7*(79), 49985–49994. https://doi.org/10.1039/c7ra08634b

Liu, Y., Tan, N., Guo, J., & Wang, J. (2020). Catalytic activation of O2 by Al0-CNTs-Cu2O composite for Fenton-like degradation of sulfamerazine antibiotic at wide pH range. *Journal of Hazardous Materials*, *396*(January), 122751. https://doi.org/10.1016/j.jhazmat.2020.122751

Liu, Y., & Wang, J. (2019). Reduction of nitrate by zero valent iron (ZVI)-based materials: A review. *Science of the Total Environment*, *671*, 388–403. https://doi.org/10.1016/j.scitotenv.2019.03.317

Liu, Y., Zhao, Y., & Wang, J. (2021). Fenton/Fenton-like processes with in-situ production of hydrogen peroxide/hydroxyl radical for degradation of emerging contaminants: Advances and prospects. *Journal of Hazardous Materials*, *404*(PB), 124191. https://doi.org/10.1016/j.jhazmat.2020.124191

Long, J., Xu, L., Zhao, L., Chu, H., Mao, Y., & Wu, D. (2020). Activation of dissolved molecular oxygen by Cu(0) for bisphenol a degradation: Role of Cu(0) and formation of reactive oxygen species. *Chemosphere*, *241*, 125034. https://doi.org/10.1016/j.chemosphere.2019.125034

Lyngsie, G., Krumina, L., Tunlid, A., & Persson, P. (2018). Generation of hydroxyl radicals from reactions between a dimethoxyhydroquinone and iron oxide nanoparticles. *Scientific Reports*, *8*(1), 2–10. https://doi.org/10.1038/s41598-018-29075-5

Mitlin, D., Beard, V. A., Satterthwaite, D., & Du, J. (2019). *Unaffordable and Undrinkable : Rethinking Urban Water Access in the Global South Una ff ordable and Undrinkable : Rethinking Urban Water Access in the Global South*.

Noubactep, C. (2009). Comment on pH dependence of fenton reagent generation and As(lll) oxidation and removal by corrosion of zero valent iron in aerated water. *Environmental Science and Technology*, *43*(1), 233. https://doi.org/10.1021/es802563j

Peng, Q., Dai, Y., Liu, K., Luo, X., He, D., Tang, X., & Huang, G. (2020). A novel carbon nanotube–magnesium oxide composite with excellent recyclability to efficiently activate peroxymonosulfate for Rhodamine B degradation. *Journal of Materials Science*, *55*(25), 11267–11283. https://doi.org/10.1007/s10853-020-04822-0

Pereira, L. S., Oweis, T., & Zairi, A. (2002). Irrigation management under water scarcity. *Agricultural Water Management*, *57*(3), 175–206. https://doi.org/10.1016/S0378-3774(02)00075-6

Physical principles of electron microscopy. (2005). *Materials Today*, *8*(12), 49. https://doi.org/10.1016/s1369-7021(05)71290-6

Pi, L., Cai, J., Xiong, L., Cui, J., Hua, H., Tang, D., & Mao, X. (2020). Generation of H2O2 by on-site activation of molecular dioxygen for environmental remediation applications: A review. *Chemical Engineering Journal*, *389*, 123420. https://doi.org/10.1016/j.cej.2019.123420

Punzi, M., Nilsson, F., Anbalagan, A., Svensson, B. M., Jönsson, K., Mattiasson, B., & Jonstrup, M. (2015). Combined anaerobic-ozonation process for treatment of textile wastewater: Removal of acute toxicity and mutagenicity. *Journal of Hazardous Materials*, *292*, 52–60.

https://doi.org/10.1016/j.jhazmat.2015.03.018

Ribeiro, M. C. M., Starling, M. C. V. M., Leão, M. M. D., & de Amorim, C. C. (2017). Textile wastewater reuse after additional treatment by Fenton's reagent. *Environmental Science and Pollution Research*, *24*(7), 6165–6175. https://doi.org/10.1007/s11356-016-6921-9

Tala-Tebue, E., Djoufack, Z. I., Fendzi-Donfack, E., Kenfack-Jiotsa, A., & Kofané, T. C. (2016). Exact solutions of the unstable nonlinear Schrödinger equation with the new Jacobi elliptic function rational expansion method and the exponential rational function method. *Optik*, *127*(23), 11124–11130. https://doi.org/10.1016/j.ijleo.2016.08.116

Tan, N., Yang, Z., Gong, X. bo, Wang, Z. ran, Fu, T., & Liu, Y. (2019). In situ generation of H2O2 using MWCNT-Al/O2 system and possible application for glyphosate degradation. *Science of the Total Environment*, *650*, 2567–2576. https://doi.org/10.1016/j.scitotenv.2018.09.353

Tchobanoglous, G., Franklin, L., Burton, E. C., & Stensel, H. D. (2011). *Wastewater Engineering Treatment and Reuse (Fourth Edition), 2011*.

The European Commission. (2003). *Integrated pollution prevention and control. Reference document on best available techniques for the textiles industry*. *July*, 626. http://eippcb.jrc.ec.europa.eu/reference/

UNEP. (2016). A Snapshot of the World ' s Water Quality : Towards a global assessment. In *United Nations Environment Programme*. https://uneplive.unep.org/media/docs/assessments/unep_wwqa_report_web.pdf

US Geological Survey. (2021). Earth's Water. In *Water Science School*. https://www.usgs.gov/special-topic/water-science-school/science

Vinila, V. S., Jacob, R., Mony, A., Nair, H. G., Issac, S., Rajan, S., Nair, A. S., Satheesh, D. J., & Isac, J. (2014). X-Ray Diffraction Analysis of Nano Crystalline Ceramic PbBaTiO₃ In *Crystal Structure Theory and Applications* (Vol. 03, Issue 03, pp. 57–65). https://doi.org/10.4236/csta.2014.33007

Wang, J. L., & Xu, L. J. (2012). Advanced oxidation processes for wastewater treatment: Formation of hydroxyl radical and application. *Critical Reviews in Environmental Science and Technology*, *42*(3), 251–325. https://doi.org/10.1080/10643389.2010.507698

Wash, R. (2002). Water security. *Water Well Journal*, *56*(3), 58. https://doi.org/10.1201/9780203878057.pt2

Wen, G., Wang, S. J., Ma, J., Huang, T. L., Liu, Z. Q., Zhao, L., & Xu, J. L. (2014). Oxidative degradation of organic pollutants in aqueous solution using zero valent copper under aerobic atmosphere condition. *Journal of Hazardous Materials*, *275*, 193–199. https://doi.org/10.1016/j.jhazmat.2014.05.002

World Population Prospects. (2022). In *World Population Prospects*. https://doi.org/10.18356/cd7acf62-en

Yang, Z., Gong, X. bo, Peng, L., Yang, D., & Liu, Y. (2018). Zn0-CNTs-Fe3O4 catalytic in situ generation of H2O2 for heterogeneous Fenton degradation of 4-chlorophenol. *Chemosphere*, *208*, 665–673. https://doi.org/10.1016/j.chemosphere.2018.06.016

Yang, Z., Gong, X., Wang, B., Yang, D., Fu, T., & Liu, Y. (2018). magnesium – carbon nanotube composites †. *RSC Advances*, *8*, 35179–35186. https://doi.org/10.1039/C8RA05907A

Yang, Z., Zhang, X., Pu, S., Ni, R., Lin, Y., & Liu, Y. (2019). Novel Fenton-like system (Mg/Fe-

O2)for degradation of 4-chlorophenol. *Environmental Pollution*, *250*, 906–913. https://doi.org/10.1016/j.envpol.2019.04.096

Yukseler, H., Uzal, N., Sahinkaya, E., Kitis, M., Dilek, F. B., & Yetis, U. (2017). Analysis of the best available techniques for wastewaters from a denim manufacturing textile mill. *Journal of Environmental Management*, *203*, 1118–1125. https://doi.org/10.1016/j.jenvman.2017.03.041

Zhang, H., Cao, B., Liu, W., Lin, K., & Feng, J. (2012). Oxidative removal of acetaminophen using zero valent aluminum-acid system: Efficacy, influencing factors, and reaction mechanism. *Journal of Environmental Sciences*, *24*(2), 314–319. https://doi.org/10.1016/S1001-0742(11)60769-9

Zhang, Y., Fan, J., Yang, B., Huang, W., & Ma, L. (2017). Copper–catalyzed activation of molecular oxygen for oxidative destruction of acetaminophen: The mechanism and superoxide-mediated cycling of copper species. *Chemosphere*, *166*, 89–95. https://doi.org/10.1016/j.chemosphere.2016.09.066